

# NATIONAL ADVISORY COMMITTEE FOR AERONAUTICS

TECHNICAL NOTE 2554

THEORETICAL AERODYNAMIC CHARACTERISTICS OF A FAMILY  
OF SLENDER WING-TAIL-BODY COMBINATIONS

By Harvard Lomax and Paul F. Byrd

Ames Aeronautical Laboratory  
Moffett Field, Calif.

**DISTRIBUTION STATEMENT A**  
Approved for Public Release  
Distribution Unlimited



Washington  
November 1951

**Reproduced From  
Best Available Copy**

20000727 086

**DTIC QUALITY INSPECTED 4**

AQM 00-10-3223

1

TABLE OF CONTENTS

	Page
SUMMARY . . . . .	1
INTRODUCTION . . . . .	1
I - SWEEP-BACK WING ON A BODY OF REVOLUTION . . . . .	2
Partial Differential Equation, Boundary Conditions, and Form of the Solution . . . . .	2
Discussion of notation and transformations . . . . .	3
Boundary conditions . . . . .	6
General solution . . . . .	6
Particular solution for the nearly constant-chord wing .	8
The Trailing Edge . . . . .	11
Special trailing-edge shape . . . . .	11
Other trailing-edge shapes . . . . .	15
The Wing Area . . . . .	16
Downwash Behind Wing . . . . .	17
Chordwise Load Distribution . . . . .	19
Loading on the wing . . . . .	19
Loading on the body . . . . .	22
Discussion of the chordwise loading . . . . .	23
Aerodynamic Characteristics . . . . .	27
Span loading . . . . .	27
Section lift . . . . .	30
Section drag . . . . .	31
Total lift . . . . .	34
Total drag . . . . .	35

Chord loading . . . . .	38
Center of pressure . . . . .	40
II - ADDITION OF A HORIZONTAL TAIL . . . . .	41
Method of Solution and Boundary Conditions . . . . .	42
Solution for Trailing Vortex Sheet . . . . .	43
Span loading . . . . .	45
Chordwise load distribution on the tail . . . . .	46
Total lift on the tail . . . . .	47
Drag . . . . .	48
Chord loading . . . . .	48
Center of pressure . . . . .	49
Solution for Rolled Up Vortices . . . . .	49
Span loading . . . . .	52
Chordwise load distribution . . . . .	53
Total lift . . . . .	53
Total drag . . . . .	54
Chord loading . . . . .	54
Center of pressure . . . . .	54
CONCLUDING REMARKS . . . . .	55
APPENDIX A . . . . .	57
APPENDIX B . . . . .	62
REFERENCES . . . . .	65
TABLES . . . . .	66
FIGURES . . . . .	69

NATIONAL ADVISORY COMMITTEE FOR AERONAUTICS

---

TECHNICAL NOTE 2554

---

THEORETICAL AERODYNAMIC CHARACTERISTICS OF A FAMILY  
OF SLENDER WING-TAIL-BODY COMBINATIONS

By Harvard Lomax and Paul F. Byrd

SUMMARY

The aerodynamic characteristics of an airplane configuration composed of a swept-back wing and a triangular tail mounted on a cylindrical body are presented. For simplicity, the leading edge of the wing is considered to be straight and the trailing edge to be shaped so that the span-loading curve is flat between the fuselage and the wing-tip regions; the result is a nearly constant-chord swept-back wing. A method by which other trailing-edge shapes can be studied is indicated. The analysis is based on the assumption that the free-stream Mach number is near unity or that the configuration is slender. The calculations for the tail are made on the assumption that the vortex system trailing back from the wing is either a sheet lying entirely in the plane of the flat tail surface or has completely "rolled up" into two point vortices that lie either in, above, or below the plane of the tail surface.

INTRODUCTION

The study of lifting surfaces flying at either subsonic or supersonic speeds at small angles of attack has been reduced, by the well-known process of linearization, to the study of the equation

$$(1-M_0^2) \phi_{xx} + \phi_{yy} + \phi_{zz} = 0 \quad (1)$$

where  $\phi$  is a perturbation velocity potential in a field having a uniform free-stream velocity  $V_0$  directed parallel to the  $x$  axis, and where  $M_0$  is the Mach number of the free stream.

One basic simplification of equation (1) is brought about by neglecting velocity gradients along the span of the wing. If the wing

is lying in the  $z = 0$  plane, this amounts to neglecting the term  $\Phi_{yy}$  in equation (1), and results in the well-known partial differential equation by means of which two-dimensional or section characteristics are studied.

Another basic simplification of equation (1) can be attained by neglecting the term  $(1-M_0^2) \Phi_{xx}$ . Such a procedure is possible when the Mach number is close to 1 or the wing plan form is so slender that velocity gradients in the free-stream direction are negligible in comparison with the gradients in the  $y$  and  $z$  directions. Equation (1) has already been analyzed in these two connections in references 1 and 2 for certain plan forms. The purpose of this report is to extend this theory, which has been named slender wing theory, to include an entire airplane configuration.

Results are presented for a nearly constant-chord, swept-back wing mounted on a cylindrical body having a triangular horizontal tail located aft of the wing trailing edge. Both wing and tail are flat surfaces, and the results are only those due to changes in the airplane angle of attack.

A list of important symbols is given in appendix A.

## I - SWEEPED-BACK WING ON A BODY OF REVOLUTION

### Partial Differential Equation, Boundary Conditions, and Form of the Solution

Under the assumption that the free-stream Mach number is 1 or that the perturbation velocity gradient in the  $x$  direction is small, the partial differential equation which must be satisfied for the solution of lifting surface problems can be written

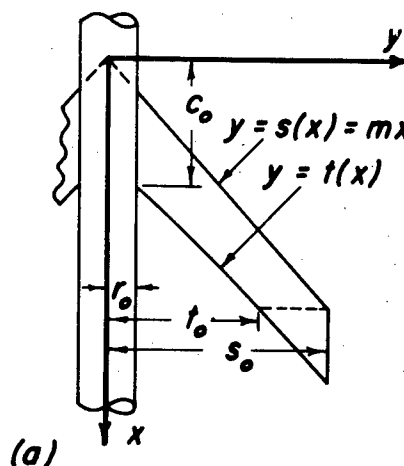
$$\Phi_{yy} + \Phi_{zz} = 0 \quad (2)$$

Equation (2) is simply Laplace's equation in two dimensions, the variables representing lateral and vertical coordinates in a plane transverse to the direction of motion.

The boundary conditions associated with equation (2) are given along a line in this transverse plane and specify that the fluid velocity is everywhere tangential to the surface of the body. The problem is, of course, to find at other points in the plane the potential that satisfies equation (2) and fits these boundary conditions. Of particular interest is the streamwise component of velocity along the surface of the wing and body since this is directly related to the loading thereon.

Solutions to equation (2) are readily available. Two different analytic forms of these solutions will be used in the following analysis. One form is concerned with the use of the complex variable, the other with the use of Green's theorem and the inversion of a real, singular, integral equation. In general the procedure will be to use concepts associated with the complex variable to map the boundary conditions onto a slit along the real axis, then to solve the resulting problem by inverting an integral equation, and finally, to use the complex variable again to extend such a solution out into space by the principle of analytic continuation.

Discussion of notation and transformations.- The first part of this report will be devoted to the analysis of the configuration shown in sketch (a). The following is a description of this configuration. Everywhere behind the leading-edge-fuselage juncture the fuselage is a circular cylinder having a radius  $r_0$ . Ahead of this juncture the fuselage comes to a point, the manner being arbitrary. The wing is a flat plate without twist or camber mounted at zero incidence on the fuselage and the whole configuration is placed at a small angle of attack  $\alpha$  with respect to the free-stream direction. The origin of the coordinate system is located at the wing apex. The leading edge is a straight line with slope,  $dy/dx$ , equal to  $m$ . It will be convenient at some places in the report, however, to use the expression  $y = s(x)$  for the equation of the leading edge, hence,  $s(x)$  and  $mx$  are used interchangeably. The trailing edge is represented by the line  $y = t(x)$  and is, in general, not straight.<sup>1</sup> The maximum semispan of the wing is denoted by  $s_0$ . The symbol  $t_0$ , as can be seen in the sketch, refers to the lateral distance from the  $x$  axis to the point at which the trailing edge intersects a line that is parallel to the  $y$  axis and passes through the last outboard point of the leading edge. Finally,  $c_0$  is the chordwise distance from the origin to the trailing-edge-fuselage juncture.



<sup>1</sup>It was considered advisable at this time to consider only the rather particular configuration outlined. As the analysis progresses it will be pointed out where the solution can be generalized to include, for example, wings with twist and camber.

A second coordinate system will also be used in the succeeding development. Let the  $y, z$  plane be represented by the complex variable  $\xi$ ,

$$\xi = y + iz = \rho e^{i\theta}$$

then introduce the  $\xi_1$  plane,

$$\xi_1 = y_1 + iz_1 = \rho_1 e^{i\theta_1}$$

so that the  $\xi$  plane maps onto the  $\xi_1$  plane by means of the Joukowski transformation

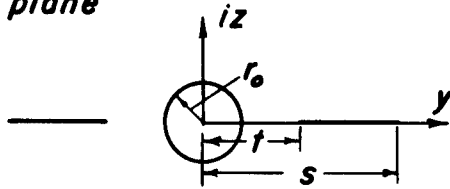
$$\xi_1 = \xi + \frac{r_0^2}{\xi} \quad (3)$$

By means of such a transformation, the circle of radius  $r_0$  which represents a section of the fuselage in the  $\xi$  plane maps onto a portion of the real axis in the  $\xi_1$  plane (see sketch (b));

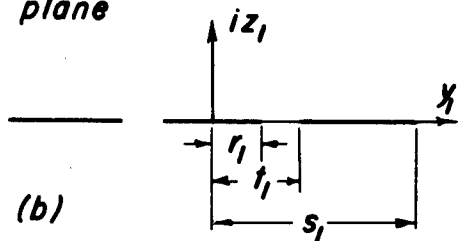
and the part of the real axis which lies outside the circle<sup>2</sup> in the  $\xi$  plane maps into the remaining part of the real axis in the  $\xi_1$  plane.

As a consequence of equation (3), the following relations hold for  $z_1$  equal to zero:

$\xi$  plane



$\xi_1$  plane



(b)

$$\left. \begin{aligned} y &= \frac{y_1 + \sqrt{y_1^2 - r_1^2}}{2}, & y_1 \geq r_1 \\ r_0 \cos \theta &= y_1/2, & -r_1 \leq y_1 \leq r_1 \\ y &= \frac{y_1 - \sqrt{y_1^2 - r_1^2}}{2}, & y_1 \leq -r_1 \end{aligned} \right\} \quad (4)$$

(4)

<sup>2</sup>The Joukowski transformation is double valued in that the regions inside and outside the circle  $\rho = r_0$  both map onto the entire  $\xi_1$  plane. In this report only the field outside the circle is of interest.

and

$$\left. \begin{aligned} y_1 &= y + \frac{r_0^2}{y}, & y_1^2 &\geq r_1^2 \\ y_1 &= 2r_0 \cos \theta, & y_1^2 &\leq r_1^2 \end{aligned} \right\} \quad (5)$$

Further,

$$s_1 = s + \frac{r_0^2}{s}, \quad t_1 = t + \frac{r_0^2}{t}, \quad r_1 = 2r_0 \quad (6)$$

From the basic theory underlying the use of complex variables in fluid-flow theory, induced velocities in the two planes are related by the expression

$$v - iw = (v_1 - iw_1) \frac{d\xi_1}{d\xi} \quad (7)$$

from which, since in polar coordinates

$$\frac{d\xi_1}{d\xi} = \left[ 1 - \left( \frac{r_0}{\rho} \right)^2 \cos 2\theta \right] + i \left( \frac{r_0}{\rho} \right)^2 \sin 2\theta \quad (8)$$

it follows that

$$\left. \begin{aligned} v &= v_1 \left[ 1 - \left( \frac{r_0}{\rho} \right)^2 \cos 2\theta \right] + w_1 \left( \frac{r_0}{\rho} \right)^2 \sin 2\theta \\ w &= w_1 \left[ 1 - \left( \frac{r_0}{\rho} \right)^2 \cos 2\theta \right] - v_1 \left( \frac{r_0}{\rho} \right)^2 \sin 2\theta \\ v_r &= \left[ v_1 \cos \theta + w_1 \sin \theta \right] \left[ 1 - \left( \frac{r_0}{\rho} \right)^2 \right] + 2w_1 \left( \frac{r_0}{\rho} \right)^2 \sin \theta \end{aligned} \right\} \quad (9)$$

Lastly, Laplace's equation must also be satisfied in the  $\xi_1$  plane, hence

$$(\phi_1)_{z_1 z_1} + (\phi_1)_{y_1 y_1} = 0 \quad (10)$$



Boundary conditions.- In this part of the report (part I), the effect of a cylindrical body mounted on a nearly constant-chord swept-back wing will be studied. (Reference 3 contains an analysis of the effect of a cylindrical body mounted on a triangular wing, and reference 4 presents results for a swept-back wing with no body; both references use the assumptions of slender-wing theory.) The boundary conditions will be presented in the  $y, z$  space first and can be written

$$\left. \begin{aligned} \text{(i)} \quad v_r &= 0, & \rho &= r_0, \quad 0 \leq \theta \leq 2\pi \\ \text{(ii)} \quad w &= 0, & z &= 0, \quad t^2 < y^2 < s^2 \\ \text{(iii)} \quad v &= 0, \quad w = V_0\alpha, & \rho &= \infty, \quad 0 \leq \theta \leq 2\pi \end{aligned} \right\} \quad (11)$$

Equations (11) represent the conditions for a cylinder located at  $\rho = r_0$  and two wing panels located between  $it$  and  $is$  on the real axis, both cylinder and wings being at rest in a free stream which is moving with velocity  $w = V_0\alpha$  at infinity.

It follows from equations (9) that these boundary conditions become, in the  $\xi_1$  plane,

$$\left. \begin{aligned} \text{(i)} \quad w_1 &= 0, & 0 < y_1^2 < r_1^2 \\ \text{(ii)} \quad w_1 &= 0, & t_1^2 < y_1^2 < s_1^2 \\ \text{(iii)} \quad v_1 &= 0, \quad w_1 = V_0\alpha, & \rho_1 &= \infty, \quad 0 \leq \theta \leq 2\pi \end{aligned} \right\} \quad (12)$$

Equations (12) represent the boundary conditions for three wing panels along the real axis, all at rest with respect to the free stream moving with velocity  $w_1 = V_0\alpha$  at infinity in the transformed plane.

It is more convenient to work with boundary conditions which vanish at infinity, however, so the final form of the conditions which must be satisfied is derived from equations (12) by subtracting the free-stream velocity  $V_0\alpha$ . There results

$$\left. \begin{aligned} \text{(i)} \quad w_1 &= -V_0\alpha, & 0 < y_1^2 < r_1^2 \\ \text{(ii)} \quad w_1 &= -V_0\alpha, & t_1^2 < y_1^2 < s_1^2 \\ \text{(iii)} \quad v_1 &= w_1 = 0, & \rho_1 &= \infty, \quad 0 \leq \theta \leq 2\pi \end{aligned} \right\} \quad (13)$$

General solution.- The general solution to equation (10) which gives the vertical induced velocity  $w_1$  at a point in the  $\xi_1$  plane due to the jump in the value of the induced velocity  $v_1$  across the  $y_1$  axis can be written (see, e.g., reference 5)

$$w_1(y_1, z_1) = - \frac{1}{2\pi} \int_{-s_1}^{s_1} \frac{(y_1 - y_2) \Delta v_1(y_2)}{(y_1 - y_2)^2 + z_1^2} dy_2 \quad (14)$$

where  $y_2$  is the variable of integration. Set  $z_1$  equal to zero and there results the value of the vertical induced velocity on the  $y_1$  axis. Thus

$$w_1(y_1) \equiv w_1(y_1, 0) = - \frac{1}{2\pi} \int_{-s_1}^{s_1} \frac{\Delta v_1(y_2)}{y_1 - y_2} dy_2 \quad (15)$$

Equation (15) is the form of the solution which will be used to analyze the problem previously outlined. It is apparent by reference to the boundary conditions listed as equations (13) that in equation (15) the value of  $w_1$  is the known quantity and  $\Delta v_1$  is the unknown. Hence, equation (15) is an integral equation which must be inverted in order that the solution can be written. Such an inversion is not difficult if the value of  $w_1$  is known everywhere in the interval  $-s_1 < y_1 < s_1$ . In the present case, however, there is a subinterval  $r_1^2 < y_1^2 < t_1^2$  in which  $w_1$  is not specified, and further, in which  $\Delta v_1$  is not necessarily zero (due to the presence of a trailing vortex sheet). It will be shown in the subsequent development that the assumption that  $\Delta v_1$  is zero in this interval (i.e., no vortices are shed by the wing ahead of the interval) yields a nearly constant-chord, swept-back wing; with such a restriction the inversion can again be performed.

Given the inversion of equation (15), it is possible to write both  $w_1$  and  $v_1$  for certain portions of the real axis. All along this axis the functions  $w_1$  and  $v_1$  are, of course, real. Hence, if

$$f(\xi_1) = v_1(y_1, z_1) - i w_1(y_1, z_1) \quad (16a)$$

then by analytic continuation

$$f(\xi_1) = v(\xi_1, 0) - i w_1(\xi_1, 0) \quad (16b)$$

Therefore, the inversion of equation (15), together with equation (16), gives sufficient information to determine the induced velocities throughout space.

Particular solution for the nearly constant-chord wing.- Adopt the notation  $\Delta v_{1b}$  equals  $\Delta v_1$  in the region of the  $y_1$  axis representing the body or fuselage in the  $\xi_1$  plane;  $\Delta v_{1a}$  equals the value of  $\Delta v_1$  in the region of the  $y_1$  axis representing the space between the fuselage and the wing; and  $\Delta v_{1w}$  equals the value of  $\Delta v_1$  in the region of the  $y_1$  axis representing the wing plan form. Then if  $\Delta v_{1a} = 0$  (the calculation of the trailing-edge shape corresponding to such a choice will be presented later), equation (15) becomes

$$w_1 = -\frac{1}{2\pi} \int_{-s_1}^{-t_1} \frac{\Delta v_{1w}}{y_1 - y_2} dy_2 - \frac{1}{2\pi} \int_{-r_1}^{r_1} \frac{\Delta v_{1b}}{y_1 - y_2} dy_2 - \frac{1}{2\pi} \int_{t_1}^{s_1} \frac{\Delta v_{1w}}{y_1 - y_2} dy_2 \quad (17)$$

Since the airplane is laterally symmetrical, the span loading is symmetrical and  $\Delta \phi_1(y_1) = \Delta \phi_1(-y_1)$ . Therefore,  $\Delta v_1$  has the property  $\Delta v_1(y_1) = -\Delta v_1(-y_1)$ . By means of this relation for  $\Delta v_1$  and the additional change in notation

$$\left. \begin{aligned} \eta_1 &= y_1^2 \\ \eta_2 &= y_2^2 \end{aligned} \right\} \quad (18)$$

equation (17) can be written

$$w_1(\eta_1) = -\frac{1}{2\pi} \int_0^{r_1^2} \frac{\Delta v_{1b} d\eta_2}{\eta_1 - \eta_2} - \frac{1}{2\pi} \int_{t_1^2}^{s_1^2} \frac{\Delta v_{1w} d\eta_2}{\eta_1 - \eta_2} \quad (19)$$

Equation (19) will now be inverted under the condition that  $w_1 = -V_0\alpha$  for  $0 < \eta_1 < r_1^2$  and for  $t_1^2 < \eta_1 < s_1^2$ , and under the additional condition that  $(\Delta v_{1w})_{\eta_2=t_1^2} = (\Delta v_{1a})_{\eta_2=t_1^2} = 0$ , which amounts to

assuming the Kutta condition along the wing trailing edge (see, e.g., reference 4). This inversion is accomplished by a double application of the following solution (see appendix B): If

$$f(\eta_1) = -\frac{1}{2\pi} \int_a^b \frac{\Delta v_1(\eta_2) d\eta_2}{\eta_1 - \eta_2} \quad (20a)$$

then, under the condition that  $\Delta v_1(a) = 0$

$$\Delta v_1(\eta_1) = \frac{2}{\pi} \sqrt{\frac{\eta_1 - a}{b - \eta_1}} \int_a^b \frac{f(\eta_2)}{\eta_1 - \eta_2} \sqrt{\frac{b - \eta_2}{\eta_2 - a}} d\eta_2 \quad (20b)$$

Now write equation (19) in the form

$$-V_0\alpha + \frac{1}{2\pi} \int_{t_1^2}^{s_1^2} \frac{\Delta v_{1w} d\eta_2}{\eta_1 - \eta_2} = - \frac{1}{2\pi} \int_0^{r_1^2} \frac{\Delta v_{1b} d\eta_2}{\eta_1 - \eta_2}$$

and then, since  $\Delta v_{1b}(0) = 0$  by reasons of symmetry, apply equation (20b). For  $0 < \eta_1 < r_1^2$ , there results the expression

$$\Delta v_{1b} = -2V_0\alpha \sqrt{\frac{\eta_1}{r_1^2 - \eta_1}} + \frac{1}{\pi} \sqrt{\frac{\eta_1}{r_1^2 - \eta_1}} \int_{t_1^2}^{s_1^2} \frac{\Delta v_{1w}}{\eta_1 - \eta_2} \sqrt{\frac{\eta_2 - r_1^2}{\eta_2}} d\eta_2 \quad (21)$$

Substitute equation (21) back into equation (19), reverse the order of integration and, for  $t_1^2 < \eta_1 < s_1^2$ , there results

$$-V_0\alpha = - \frac{1}{2\pi} \sqrt{\frac{\eta_1}{\eta_1 - r_1^2}} \int_{t_1^2}^{s_1^2} \frac{g(\eta_2) d\eta_2}{\eta_1 - \eta_2} \quad (22)$$

where

$$g(\eta_2) = \Delta v_{1w}(\eta_2) \sqrt{\frac{\eta_2 - r_1^2}{\eta_2}} \quad (23)$$

Again apply equation (20b), this time to equation (22). In this way  $g(\eta_1)$  can be shown to satisfy the relation

$$g(\eta_1) = -2V_0\alpha \sqrt{\frac{\eta_1 - t_1^2}{s_1^2 - \eta_1}} \quad (24)$$

and equating this expression to equation (23) gives

$$\Delta v_{1w} = -2V_0\alpha \sqrt{\frac{\eta_1(\eta_1 - t_1^2)}{(s_1^2 - \eta_1)(\eta_1 - r_1^2)}}, \quad t_1^2 < \eta_1 < s_1^2 \quad (25a)$$

A repetition of the above process yields<sup>3</sup>

$$\Delta v_{1b} = -2V_0\alpha \sqrt{\frac{\eta_1(t_1^2 - \eta_1)}{(s_1^2 - \eta_1)(r_1^2 - \eta_1)}}, \quad 0 < \eta_1 < r_1^2 \quad (25b)$$

The results given by equations (25) can be extended to other points in space by analytic continuation. Equations (16) indicate the necessary procedure. Hence, since  $(v_1)_{z_1=0} = \Delta v_1/2$ ,

$$v_1(y_1, z_1) - iw_1(y_1, z_1) = V_0\alpha \left[ i + \sqrt{\frac{\xi_1^2(\xi_1^2 - t_1^2)}{(s_1^2 - \xi_1^2)(\xi_1^2 - r_1^2)}} \right] \quad (26)$$

---

<sup>3</sup>When the method is applied to a value of  $w_1$  which has some given variation with  $\eta_1$  there results

$$\Delta v_{1b}(\eta_1) = \frac{2}{\pi} \sqrt{\frac{\eta_1(t_1^2 - \eta_1)}{(r_1^2 - \eta_1)(s_1^2 - \eta_1)}} \left[ \int_0^{r_1^2} \frac{w_1(\eta_2)}{\eta_1 - \eta_2} d\eta_2 \sqrt{\frac{(s_1^2 - \eta_2)(r_1^2 - \eta_2)}{\eta_2(t_1^2 - \eta_2)}} + \int_{t_1^2}^{s_1^2} \frac{w_1(\eta_2)}{\eta_1 - \eta_2} d\eta_2 \sqrt{\frac{(\eta_2 - r_1^2)(s_1^2 - \eta_2)}{\eta_2(\eta_2 - t_1^2)}} \right], \quad 0 < \eta_1 < r_1^2$$

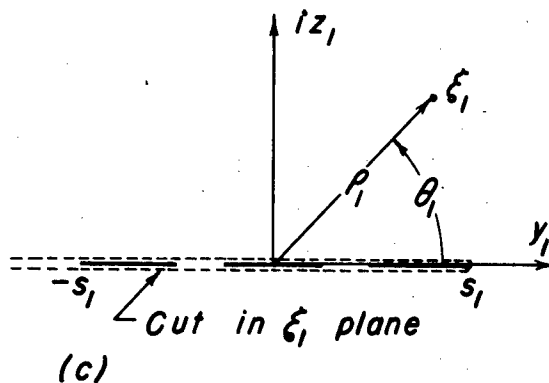
and

$$\Delta v_{1w}(\eta_1) = \frac{2}{\pi} \sqrt{\frac{\eta_1(\eta_1 - t_1^2)}{(s_1^2 - \eta_1)(\eta_1 - r_1^2)}} \left[ \int_0^{r_1^2} \frac{w_1(\eta_2)}{\eta_1 - \eta_2} d\eta_2 \sqrt{\frac{(r_1^2 - \eta_2)(s_1^2 - \eta_2)}{\eta_2(t_1^2 - \eta_2)}} + \int_{t_1^2}^{s_1^2} \frac{w_1(\eta_2)}{\eta_1 - \eta_2} d\eta_2 \sqrt{\frac{(\eta_2 - r_1^2)(s_1^2 - \eta_2)}{\eta_2(\eta_2 - t_1^2)}} \right], \quad t_1^2 < \eta_1 < s_1^2$$


---

Equation (26) has several branch points so it is not uniquely defined without specifying the cut from  $-\infty$  to  $s_1$  along the real axis in the  $\xi_1$  plane (see sketch (c)).

In the upper half of the  $\xi_1$  plane  $\theta_1$  varies between 0 and  $\pi$  and in the lower half, between 0 and  $-\pi$ . Notice that when  $\xi_1$  is at a very large distance from the origin in any direction the magnitude of the term on the right-hand side of equation (26) tends to zero, so that the boundary conditions at infinity are satisfied. It is evident that the other boundary conditions in equations (13) are also satisfied.

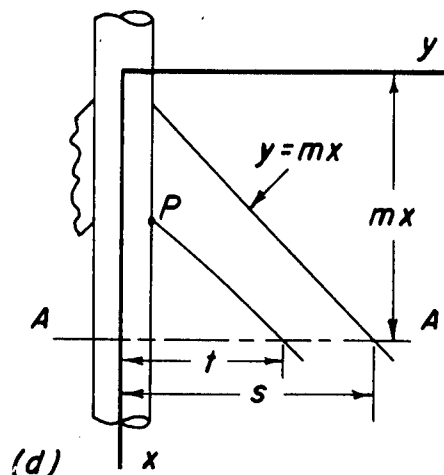


#### The Trailing Edge

Special trailing-edge shape.— Equation (26) is a solution to Laplace's equation and represents the flow around a wing and body. However, the plan form of the wing has not as yet been evaluated, although it has been fixed as that which makes the value of  $\Delta v_1$  vanish in the region between the wing and the body. Since  $\Delta v_1$  is the gradient of  $\Delta \phi_1$  in the  $y_1$  direction, and further, since  $(\Delta \phi_1)_{T.E.}$  (the value of  $\Delta \phi_1$  at the wing trailing edge) equals the total circulation  $\Gamma_1$  about a given chordwise section, this amounts to the same thing as assuming that there are no trailing vortices between the wing and the body. It is a further consequence of such an assumption that the span loading ahead of this region is a constant for  $r_0^2 < y_0^2 < t_0^2$ . The configuration which will produce such a flow must now be determined. In particular, if the leading edge is taken to be a straight line, the equation for the trailing edge is unique and needs to be expressed.

One of the simplest ways of finding the shape of the trailing edge is to find  $\Delta \phi_{T.E.}$  from equation (26) and solve for  $t$  as a function

of  $s$  for a fixed value of  $r_0$  and  $\Delta\phi_{T.E.}$ . The constant representing  $\Delta\phi_{T.E.}$  is the value of the jump in potential at the point  $P$  in sketch (d). Here  $\Delta\phi$  is known (see, e.g., reference 3) since there is no gap to make its solution indeterminate.



Consider an arbitrary section, as AA in sketch (d), downstream of the point  $P$ . The value of  $\Delta\phi_{1w}$  at such a section is given by equation (25a) and the solution for  $\Delta\phi_{1w}$  follows by definition and is

$$\Delta\phi_{1w} = -2V_0\alpha \int_{s_1}^{y_1} y_2 \sqrt{\frac{y_2^2 - t_1^2}{(s_1^2 - y_2^2)(y_2^2 - r_1^2)}} dy_2 \quad (27)$$

Equation (27) is an elliptic integral which can be easily reduced by means of the substitutions

$$k_1^2 = \frac{s_1^2 - t_1^2}{s_1^2 - r_1^2}, k_1'^2 = \frac{t_1^2 - r_1^2}{s_1^2 - r_1^2} \quad (28)$$

and by using the Jacobian elliptic functions defined, in this case, by

$$(s_1^2 - t_1^2) \operatorname{sn}^2 u = s_1^2 - y_1^2, \operatorname{cn}^2 u = 1 - \operatorname{sn}^2 u, \operatorname{dn}^2 u = 1 - k_1^2 \operatorname{sn}^2 u$$

to the form

$$\Delta\phi_{1w} = 2V_0\alpha \sqrt{s_1^2 - r_1^2} \left[ E(k_1, \psi_1) - k_1'^2 F(k_1, \psi_1) \right] \quad (29)$$

where

$$\psi_1 = \sqrt{\frac{s_1^2 - y_1^2}{s_1^2 - t_1^2}} \quad (30)$$

and where the incomplete elliptic integrals  $E$  and  $F$  are defined in the list of symbols (appendix A). Equation (29) reduces to the results given in references 3 and 4 when there is no gap or no body, respectively.

At the trailing edge  $y_1 = t_1$ , and equation (29) becomes

$$(\Delta\phi_1)_{T.E.} = 2V_0\alpha \sqrt{s_1^2 - r_1^2} \left( E_{1-k_1'^2} K_1 \right) \quad (31)$$

where the elliptic integrals are now complete. Transform this to the physical plane, using equation (6), and set

$$k_0 = \frac{\sqrt{(s^2 t^2 - r_0^2)(s^2 - t^2)}}{t(s^2 - r_0^2)}, \quad k_0' = \sqrt{1 - k_0^2} \quad (32)$$

then there results

$$\Delta\phi_{T.E.} = 2V_0\alpha \left( \frac{s^2 - r_0^2}{s} \right) \left( E_{0-k_0'^2} K_0 \right) \quad (33a)$$

At the juncture of the fuselage and the wing trailing edge (the point P in sketch (d)),  $s$  equals  $mc_0$  and  $t$  equals  $r_0$ , so that equation (33a) reduces to

$$(\Delta\phi)_{T.E.} = 2V_0\alpha mc_0 \left[ 1 - \left( \frac{r_0}{mc_0} \right)^2 \right] \quad (33b)$$

As was pointed out, the solution for the equation of the trailing edge can be obtained by equating these two values of  $(\Delta\phi)_{T.E.}$ . Hence

$$mc_0 \left[ 1 - \left( \frac{r_0}{mc_0} \right)^2 \right] = \frac{s^2 - r_0^2}{s} \left( E_{0-k_0'^2} K_0 \right)$$

or

$$t^2 - mc_0 t \left\{ \frac{\left[ 1 - \left( \frac{r_0}{mc_0} \right)^2 \right] k_0'}{E_{0-k_0'^2} K_0} \right\} - r_0^2 = 0 \quad (34)$$

Set

$$G = mc_0 \frac{\left[ 1 - \left( \frac{r_0}{mc_0} \right)^2 \right] k_0'}{E_{0-k_0'^2} K_0}$$



and since  $s$  equals  $mx$

$$k_0' = \left( \frac{t^2 - r_0^2}{m^2 x^2 - r_0^2} \right) \frac{mx}{t}$$

From equation (34) the solution that gives the correct trailing-edge shape can be written

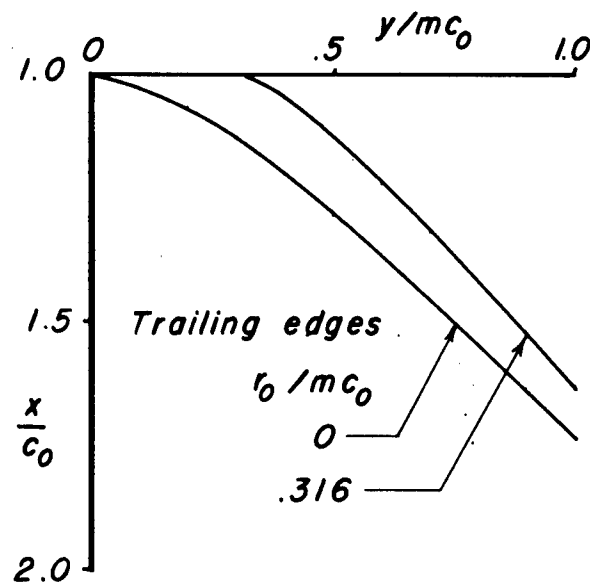
$$t = \frac{G + \sqrt{G^2 + 4r_0^2}}{2} \quad (35)$$

and from the definition of  $k_0'$

$$mx = \frac{t^2 - r_0^2 + \sqrt{(t^2 - r_0^2)^2 + 4k_0'^2 t^2 r_0^2}}{2k_0' t} \quad (36)$$

If  $k_0'$  and  $r_0/mc_0$  are fixed,  $t/mc_0$  is determined from equation (35); and a fixed  $k_0'$ ,  $r_0/mc_0$  and  $t/mc_0$  determines  $x/c_0$  from equation (36). Hence, it is relatively easy to calculate numerically the shape of the trailing edge.

Sketch (e) shows the shape and position of the trailing edge when the wing leading edge is swept back  $45^\circ$  and the radius of the fuselage is 31.6 percent of the extended root chord,  $c_0$ . (A dimensionless



coordinate system is chosen, however, so that the results can be used for various values of  $m$  and  $c_0$ .) Shown also, for comparative purposes, is the position of the trailing edge when there is no fuselage - the condition in both cases being, of course, that no vortices trail back in the region directly behind the wing. Table 1 presents coordinates of the trailing edge for several values of  $r_0/mc_0$ .

(e)

Sketch (f) indicates the variation of the local chord along the span for  $r_0/mc_0$  equal to 0.6, 0.316, and 0. It is apparent that the effect of the body is to make the trailing edge more nearly that of a constant-chord wing. The asymptotic value of the wing chord is given by the equation

$$\frac{c_\infty}{c_0} = \frac{2}{\pi} \left[ 1 - \left( \frac{r_0}{mc_0} \right)^2 \right] \quad (37)$$

where

$$c_\infty = \lim_{x \rightarrow \infty} \left( x - \frac{t}{m} \right)$$

More complete results are given in table 2.

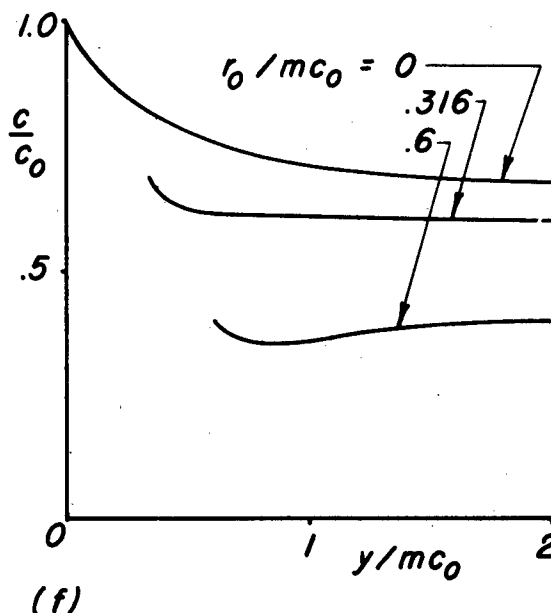
Other trailing-edge shapes.— The procedure just presented can be generalized and used to calculate trailing-edge shapes corresponding to arbitrary span-loading curves. Suppose that the span loading in the transformed (or  $\xi_1$ ) plane is represented by a power series in  $y_1$  in the interval  $r_1^2 \leq y_1^2 \leq t_1^2$ . Then the circulation in this interval can be written

$$\Gamma(y_1) = \sum_{n=0}^m b_n y_1^n$$

and, hence,  $\Delta v_{1a}$ , the value of  $\Delta v_1$  in the same interval, becomes

$$\Delta v_{1a} = \sum_{n=0}^m n b_n y_1^{n-1}$$

Equation (19) now takes the form



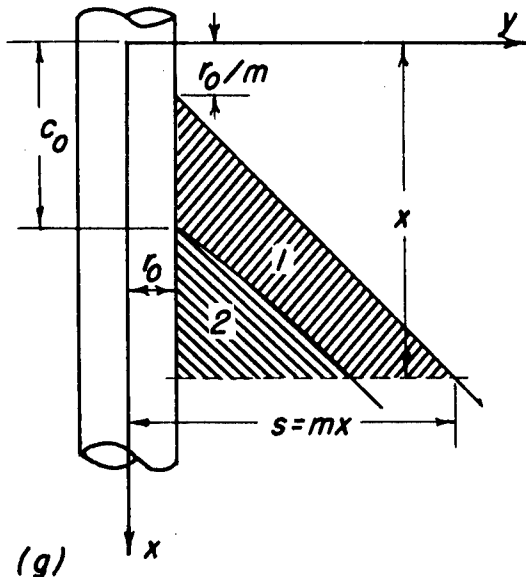
$$w_1 + \frac{1}{2\pi} \int_{r_1^2}^{t_1^2} \frac{\Delta v_{1a} d\eta_2}{\eta_1 - \eta_2} = - \frac{1}{2\pi} \int_0^{r_1^2} \frac{\Delta v_{1b} d\eta_2}{\eta_1 - \eta_2} - \frac{1}{2\pi} \int_{t_1^2}^{s_1^2} \frac{\Delta v_{1w} d\eta_2}{\eta_1 - \eta_2}$$

The left-hand side of the latter equation varies with  $\eta_1$  in a given manner depending on the  $b_n$ 's in the expression for  $\Gamma$ . Hence, the equation can be considered as identical to equation (19), the left side being regarded as an effective  $w_1$  in equation (19). The analysis succeeding equation (19) can now be repeated in terms of the equivalent  $w_1$ . There results an equation for the trailing edge which depends on the  $b_n$ 's.

By the process outlined, both the trailing-edge shape and the span-loading curve have been expressed in terms of  $m+1$  constants. By varying the number and magnitude of these constants, a large class of trailing-edge shapes can be obtained.

#### The Wing Area

Having found the shape of the trailing edge by the methods outlined in the preceding section, it is now possible to determine the area of the wing. Denote this area, region 1 in sketch (g), as  $S_1$  and the area of region 2, shown also in the sketch, as  $S_2$ . It is evident that the sum of these two areas is simply



$$S_1 + S_2 = \frac{1}{2} (mx - r_0) \left( x - \frac{r_0}{m} \right) = \frac{m}{2} \left( x - \frac{r_0}{m} \right)^2$$

Replace  $S_2$  by its integral equivalent and there results

$$S_1 = \frac{m}{2} \left( x - \frac{r_0}{m} \right)^2 - \int_{c_0}^x dx \int_{r_0}^{t(x)} dy$$

If a dimensionless system based on the length  $c_0$  is adopted, one can write for the total area (i.e., both panels, see the shaded area in sketch (h1)) of the wing the equation

$$\frac{S}{mc_0^2} = \left(\frac{x}{c_0}\right)^2 + \left(\frac{r_0}{mc_0}\right)^2 - 2 \frac{r_0}{mc_0} - 2 \int_1^{x/c_0} \frac{t}{mc_0} d\left(\frac{x}{c_0}\right)$$

where  $t/mc_0$  is given numerically as a function of  $x/c_0$  in table 1 ( $y/mc_0$  in the table representing  $t/mc_0$ ). Numerical relations between the parameters  $S/mc_0^2$ ,  $r_0/mc_0$ ,  $s_0/mc_0$ , and  $t_0/s_0$  are presented in figure 1.

The area of a wing with another kind of tip shape can be readily evaluated once the particular tip shape is specified. For example, the area of the wing shown in sketch (h2) can be calculated by subtracting a rectangular area (given by the sum of the two triangular regions labeled 3 in sketch (h2)) from the area of a sketch (h1).

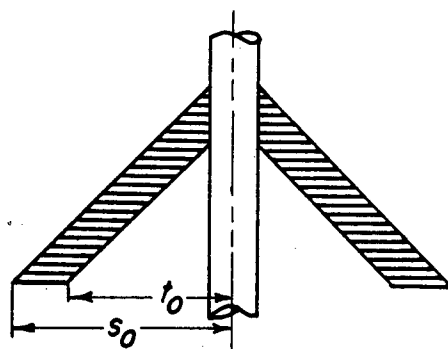
#### Downwash Behind Wing

The equation for the downwash behind the wing and in the  $z = 0$  plane follows immediately from equation (26). In the transformed  $\xi_1$  plane the value of  $w_1$  is

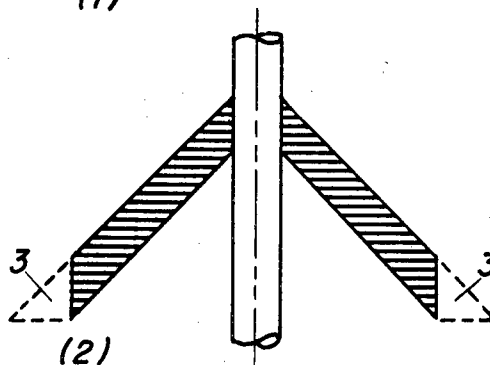
$$w_1 = -V_0\alpha, \quad 0 < y_1^2 < r_1^2; t_1^2 < y_1^2 < s_1^2 \quad (38a)$$

and

$$w_1 = -V_0\alpha \left[ 1 - \sqrt{\frac{y_1^2(t_1^2 - y_1^2)}{(s_1^2 - y_1^2)(y_1^2 - r_1^2)}} \right], \quad r_1^2 < y_1^2 < t_1^2 \quad (38b)$$



(1)



(2)

(h)

In order to transform this value to the physical plane, care must be taken to go backwards through the boundary conditions in the proper order. Equations (38) represent the solution for the boundary conditions presented in equation (13). To find the solution for the conditions given by equation (12) a free stream  $V_0\alpha$  must be added. Thus, in mathematical notation,

$$(w_1)_{12} = (w_1)_{13} + V_0\alpha$$

where the subscripts 12 and 13 refer to the boundary conditions satisfied. Finally, to find the downwash in the physical plane, the transformations given as equations (9) and (5) must be employed and the free stream subtracted so that

$$w(y) = \left[ (w_1)_{13} + V_0\alpha \right] \frac{y^2 - r_0^2}{y^2} - V_0\alpha$$

where  $(w_1)_{13}$  now becomes

$$(w_1)_{13} = -V_0\alpha, \quad 0 < y^2 < r^2; t^2 < y^2 < s^2$$

and

$$(w_1)_{13} = -V_0\alpha \left[ 1 - \frac{y^2 + r_0^2}{y^2 - r_0^2} \left( \frac{s}{t} \right) \sqrt{\frac{(y^2 t^2 - r_0^4)(t^2 - y^2)}{(s^2 y^2 - r_0^4)(s^2 - y^2)}} \right], \quad r^2 < y^2 < t^2$$

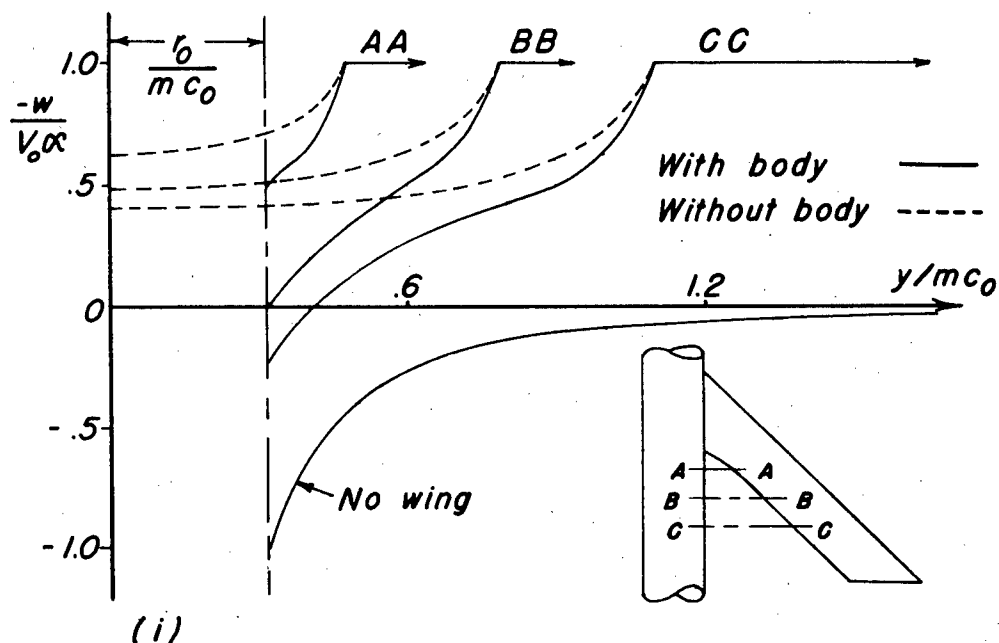
Combining and simplifying, one finds

$$w(y) = -V_0\alpha, \quad 0 < y^2 < r^2; t^2 < y^2 < s^2 \quad (39a)$$

and

$$w(y) = -V_0\alpha \left[ 1 - \frac{y^2 + r_0^2}{y^2} \left( \frac{s}{t} \right) \sqrt{\frac{(y^2 t^2 - r_0^4)(t^2 - y^2)}{(s^2 y^2 - r_0^4)(s^2 - y^2)}} \right], \quad r^2 < y^2 < t^2 \quad (39b)$$

The accompanying sketch shows the variation of  $-w/V_0\alpha$  in the intervals for which it has been given. If no wing is attached to the



body (or if the gap is very large) the fluid at the side of the body is moving upward at a speed equal to that at which the body is moving downward. The presence of the wing restricts this motion and as the wing panel approaches the body the air in the gap is forced more and more to move downward with the wing and body. The dotted lines in the sketch show the variation of  $-w/V_0\alpha$  if no body is present, that is, if  $r_0$  equals zero.

#### Chordwise Load Distribution

Loading on the wing.— The loading on the wing can be calculated by means of the linearized equation for the loading coefficient. This equation can be written

$$\left(\frac{\Delta p}{q}\right)_w = \frac{2\Delta u}{V_0} = \frac{2}{V_0} \frac{\partial \Delta \Phi_w}{\partial x} \quad (40a)$$

It is somewhat easier to calculate the loading if the derivative of  $\Delta\phi_w$  is taken in the  $\xi_1$  plane. If  $\Delta\phi_{1w}$  is considered to be a function of the two independent variables  $y_1$  and  $s_1$ , equation (40a) can be modified slightly to read

$$\left(\frac{\Delta p}{q}\right)_w = \frac{2}{V_0} \frac{\partial \Delta\phi_{1w}}{\partial s_1} \frac{ds_1}{ds} \frac{ds}{dx} \quad (40b)$$

The value of  $\frac{\partial \Delta\phi_{1w}}{\partial s_1}$  can be obtained by differentiating equation (29), thus

$$\begin{aligned} \frac{\partial \Delta\phi_{1w}}{\partial s_1} = 2V_0\alpha \left\{ \frac{s}{\sqrt{s_1^2 - r_1^2}} \left[ E(k_1, \psi_1) - k_1'^2 F(k_1, \psi_1) \right] + \right. \\ \left. \sqrt{s_1^2 - r_1^2} \left[ \frac{\partial E(k_1, \psi_1)}{\partial s_1} - k_1'^2 \frac{\partial F(k_1, \psi_1)}{\partial s_1} - 2k_1' F(k_1, \psi_1) \frac{dk_1'}{ds_1} \right] \right\} \end{aligned}$$

which becomes

$$\begin{aligned} \frac{\partial \Delta\phi_{1w}}{\partial s_1} = 2V_0\alpha \left\{ \frac{s}{\sqrt{s_1^2 - r_1^2}} \left[ E(k_1, \psi_1) - k_1'^2 F(k_1, \psi_1) \right] + \right. \\ \left. \sqrt{s_1^2 - r_1^2} \left[ \left( F(k_1, \psi_1) + \psi_1 \sqrt{\frac{1 - \psi_1^2}{1 - k_1^2 \psi_1^2}} \right) k_1 \frac{dk_1}{ds_1} + k_1'^2 \sqrt{\frac{1 - \psi_1^2}{1 - k_1^2 \psi_1^2}} \frac{\partial \psi_1}{\partial s_1} \right] \right\} \quad (41) \end{aligned}$$

The terms  $dk_1/ds_1$  and  $\partial\psi_1/\partial s_1$  both involve  $dt_1/ds_1$  which is proportional to the slope of the trailing edge in the transformed  $\xi_1$  plane. This latter derivative can be readily obtained from equation (41) itself since the value of  $(\Delta p/q)_w$  and hence  $\partial\Delta\phi_{1w}/\partial s_1$  must be zero on the trailing edge, that is, where  $y_1$  equals  $t_1$  and  $\psi_1$  equals 1. This yields the relation

$$\frac{dt_1}{ds_1} = \frac{s_1 E_1}{t_1 K_1} \quad (42)$$

by means of which the identities

$$\left. \begin{aligned} \frac{\partial \psi_1}{\partial s_1} &= \frac{s_1}{s_1^2 - r_1^2} \left( \frac{\psi_1 E_1}{k_1^2 K_1} + \frac{1 - \psi_1^2}{\psi_1 k_1^2} \right) \\ \text{and} \quad k_1 \frac{dk_1}{ds_1} &= \frac{-s_1}{s_1^2 - r_1^2} \left( \frac{E_1 - k_1'^2 K_1}{K_1} \right) \end{aligned} \right\} \quad (43)$$

can be written. Place equations (41) and (43) into equation (40b), and there results for the loading

$$\frac{1}{m} \left( \frac{\Delta p}{q\alpha_w} \right) = 4 \frac{s_1}{\sqrt{s_1^2 - r_1^2}} \left[ E(k_1, \psi_1) - \frac{E_1}{K_1} F(k_1, \psi_1) + \frac{1}{\psi_1} \sqrt{(1 - \psi_1^2)(1 - k_1'^2 \psi_1^2)} \right]$$

Transforming this to the  $\xi$  plane, one finds, finally, since  $ds_1/ds = (s^2 - r_0^2)/s^2$

$$\frac{1}{m} \left( \frac{\Delta p}{q\alpha_w} \right) = 4 \frac{s^2 + r_0^2}{s^2} \left[ E(k_0, \psi_0) - \frac{E_0}{K_0} F(k_0, \psi_0) + \frac{s^2(y^2 - r_0^2)}{yt(s^2 - r_0^2)} \sqrt{\frac{(y^2 - t^2)(y^2 t^2 - r_0^4)}{(s^2 - y^2)(s^2 y^2 - r_0^4)}} \right] \quad (44)$$

where  $k_0$  is defined by equation (33) and

$$\psi_0 = \frac{t}{y} \sqrt{\frac{(s^2 - y^2)(s^2 y^2 - r_0^4)}{(s^2 - t^2)(s^2 t^2 - r_0^4)}} \quad (45)$$

In the special cases when there is no body or when the wing is triangular, equation (44) agrees with the results presented in references (4) and (3), respectively. A discussion of the chordwise load distribution over the wing will be given at the end of this section.



Loading on the body.- The variation of the load distribution over the body can be calculated in much the same way as that over the wing. It is first necessary, therefore, to find the jump in potential between points directly opposed above and below the  $z = 0$  plane. In the  $\xi_1$  plane this difference follows immediately from equation (25b) just as equation (27) was written for  $\Delta\Phi_{1w}$ . Hence,

$$\Delta\Phi_{1b} = - 2V_0\alpha \int_{s_1}^{t_1} y_2 \sqrt{\frac{y_2^2 - t_1^2}{(s_1^2 - y_2^2)(y_2^2 - r_1^2)}} dy_2 - 2V_0\alpha \int_{r_1}^{y_1} y_2 \sqrt{\frac{t_1^2 - y_2^2}{(s_1^2 - y_2^2)(r_1^2 - y_2^2)}} dy_2 \quad (46)$$

The first of the integrals in equation (46) has already been evaluated and the second can be reduced by means of the transformation

$$(t_1^2 - y_2^2) \operatorname{sn}^2 u = r_1^2 - y_2^2$$

After some manipulation, equation (46) becomes

$$\Delta\Phi_{1b} = 2V_0\alpha \left[ E_1 - E(k_1, \psi_3) + k_1'^2 F(k_1, \psi_3) - k_1'^2 K_1 \right] \sqrt{s_1^2 - r_1^2} + 2V_0\alpha \sqrt{\frac{(s_1^2 - y_1^2)(r_1^2 - y_1^2)}{t_1^2 - y_1^2}} \quad (47)$$

where  $k_1$  is defined by equation (28) and

$$\psi_3 = \sqrt{\frac{r_1^2 - y_1^2}{t_1^2 - y_1^2}} \quad (48)$$

Using the equations (42) and (47), one can write for the loading on the body (after differentiation and simplification of equation (47))

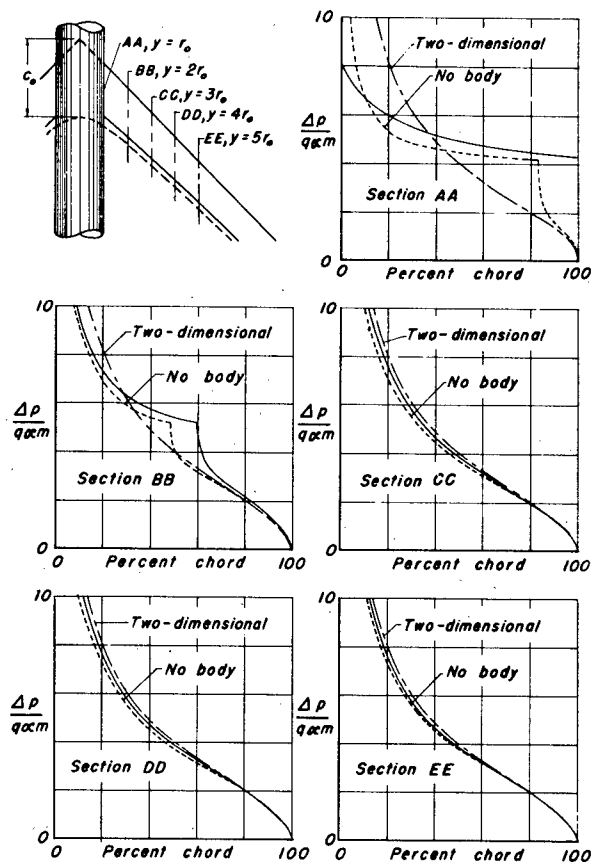
$$\frac{1}{m} \left( \frac{\Delta p}{q\alpha} \right)_b = 4 \left( \frac{s^2 + r_o^2}{s^2} \right) \left\{ \frac{E_o}{K_o} F(k_o, \psi_2) - E(k_o, \psi_2) + \frac{2k_o^2(s^2 - r_o^2)t}{\sqrt{[(t^2 + r_o^2)^2 - 4y^2t^2][(s^2 + r_o^2)^2 - 4y^2s^2]}} \right\} \quad (49)$$

where  $k_o$  is defined by equation (33) and

$$\psi_2 = 2t \sqrt{\frac{r_o^2 - y^2}{(t^2 + r_o^2)^2 - 4y^2t^2}} \quad (50)$$

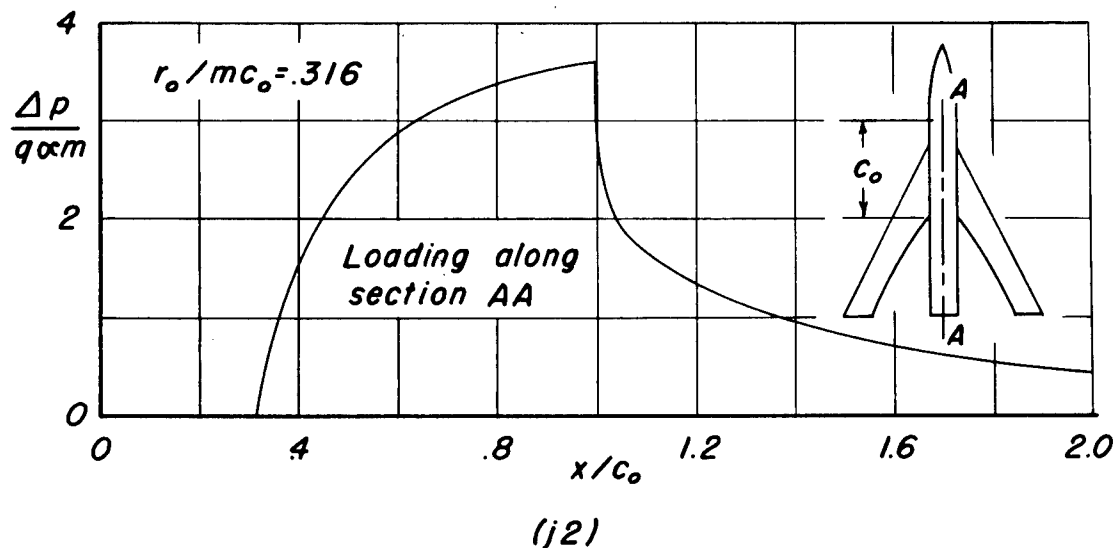
Again equation (49) agrees with previously known results in the limiting cases when the body vanishes or when the wing becomes triangular.

Discussion of the chord-wise loading.— Equations (44) and (49) form the basic results of part I of this report. Graphs of the loading coefficient for a wing alone and for a wing-body combination ( $r_o/mc_o$  equals 0.316) are shown in sketch (j1). The results for the case of zero body radius could have been obtained directly from reference 4. They are shown here for the purpose of a qualitative comparison. Unfortunately, the load distributions on the two wings cannot be compared quantitatively on the basis of equivalent plan forms since the trailing-edge shapes differ significantly. The variation



(j1)

of the loading along the center line of the body is shown in sketch (j2).



On the basis of the load distributions presented in references 3 and 4, the qualitative variation of loading shown in sketch (j1) is obvious. That is, the loading falls steadily from its infinite peak at the leading edge to zero at the trailing edge. On sections which are cut by the Mach wave from the trailing-edge fuselage juncture, the slope of the curve is discontinuous.

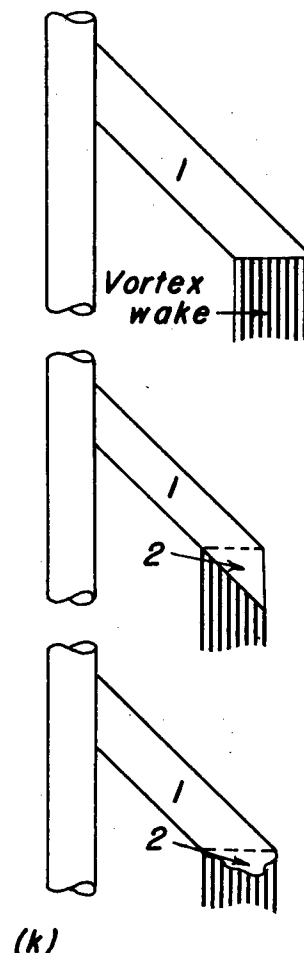
The change in the load distribution brought about by the presence of a wing tip is the same for a wing-body combination as for a wing alone. The behavior of the loading in the vicinity of a tip has a straightforward explanation in terms of the trailing vortex sheet. Thus, if the wing is cut off along a line perpendicular to the free-stream direction, the vortices which were bound in the wing all turn and trail backwards with the same distribution in strength<sup>4</sup> as they had when

---

<sup>4</sup>This assumes, of course, that the vortices have not begun to roll up to any significant extent.

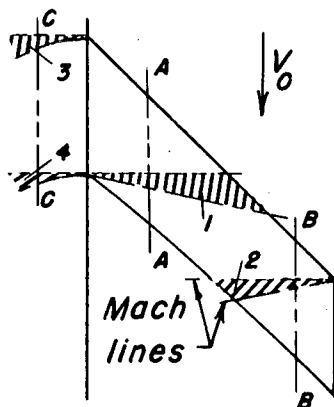
crossing the last spanwise section of the wing (see sketch (k)). Since the vertical induced velocity along the last spanwise section was made constant (by finding the appropriate solution to the integral equation), it must also be constant - and, in fact, the same constant - everywhere in the vortex wake. Hence, if a flat surface having the same angle of attack as the wing is inserted anywhere in the wake it will in no way disturb the flow and consequently there will be no loading on such a surface (just as there is no loading on the vortex wake itself). The loading is zero, therefore, on the tip regions marked 2 in sketch (k); the loading in the regions marked 1 being given, of course, by equation (44).

It is interesting to see how the distribution and magnitude of the loading given by this (slender wing) theory compare with linearized theory results at some Mach number other than 1. The differences caused by considering Mach numbers other than 1 depend, of course, on whether or not the new Mach number is subsonic or supersonic. This discussion must be limited to a comparison with supersonic Mach numbers only, since theoretical chordwise load distributions over swept-back wings flying at high subsonic speeds are not available. The change in the loading brought about by increasing the speed can be divided into two parts: one, a change caused by the rotation of the Mach lines which form the boundaries of the various regions in each of which the shape of the loading curve takes widely different forms; and the other, a change in the magnitude of the loading within each of these regions.



Sketch (l) indicates these effects. Thus, on the wing flying at supersonic speeds the sharp drop in loading occurring at a critical Mach line moves farther back along the chord from point b to point a in sections AA and BB shown in the sketch. This causes a considerably higher value of the loading for the supersonic wing<sup>5</sup> in regions 1 and 2. A similar effect occurs on the body traveling at a supersonic speed where now, however, the traces of the Mach lines are no longer straight but,

<sup>5</sup>Solutions showing the effect of crossing critical Mach lines on a swept-back supersonic wing are given in references 6 and 7.



due to the curvature of the body, form helices. Region 3 in the supersonic case would be a region of zero loading and region 4 would be a region of high loading relative to the sonic value.

The relative magnitude of  $\Delta p/q\alpha$  within the various areas bounded by the wing edges and the pertinent Mach lines changes as the reference section moves outboard along the wing span. Along inboard sections ahead of region 1 in the sketch (i.e., ahead of the sonic Mach line from the trailing edge root) the loading on the sonic wing is higher than that on the supersonic wing. It is well known, for example, that in the case of a triangular wing without body, slender-wing theory gives a loading  $E$  times the loading obtained at a supersonic Mach number (where  $E$  is the complete elliptic integral of the

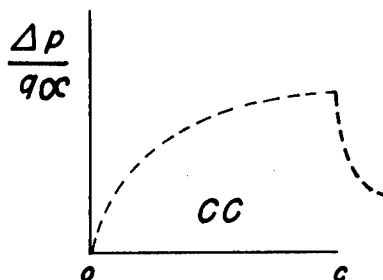
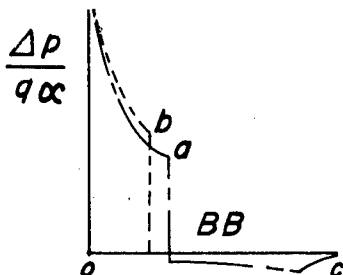
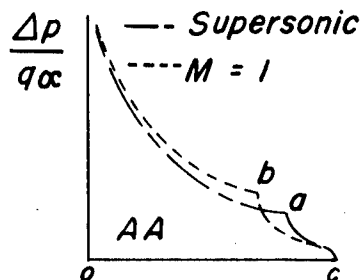
second kind with modulus  $\sqrt{1-m^2\beta^2}$  and is given

closely by  $1 + \frac{1}{2} m^2\beta^2 \left( \ln \frac{4}{m\beta} - \frac{1}{2} \right)$  for

small values of  $m\beta$ ). On the other hand, along sections farther outboard, the magnitude of  $\Delta p/q\alpha$  on the sonic wing must become lower than that on the supersonic wing. This follows immediately from simple sweep theory, since the component of velocity normal to the leading edge is closer to the speed of sound than that for the sonic wing. In fact, it is easy to show that at distances far enough outboard so that simple sweep theory applies<sup>6</sup> the supersonic wing has a loading

$(1 - m^2\beta^2)^{-1/2}$  times that obtained from slender wing theory.

By an application of the above considerations, it is possible to obtain an estimate of the absolute value of the loading on a wing-body combination at supersonic Mach



(1)

<sup>6</sup>Sketch (j1) indicates the manner in which the loading approaches that given by simple sweep theory as the reference station moves outboard.

numbers. Another manner in which the results of slender wing theory can be extended to Mach numbers other than 1 (or to plan forms which are not sufficiently slender) is to form the ratio of the resulting values for the wing plus body to those for the wing alone and apply this ratio to solutions for the same wing or body at the required flight Mach numbers (or slenderness factor). As has already been mentioned, the formation of such a ratio for the load distribution is not possible from the solutions presented herein since the wing trailing edges change to a certain extent with the addition of the body. It is reasonable to expect, however, that a ratio of the integrated loading characteristics (i.e., lift, drag, and pitching moment) formed by dividing the result for a wing-body combination by those for a wing alone will be useful in estimating the interference effects even if the wing trailing edges differ slightly.

#### Aerodynamic Characteristics

The results developed in the preceding section can now be converted into forms which represent the aerodynamic characteristics of the wing and body. Hence, the following will present the span loading, average chord loading, lift, drag, pitching moment, and center of pressure for the wing-body combination.

Span loading.— The development of the span loading on the wing and body will be considered separately. First the span loading on the wing can easily be determined from the value of  $\Delta\phi$  given in a preceding section. Thus

$$\frac{L_w}{q} = \iint_{\text{wing plan form}} \frac{\Delta p}{q} dy dx$$

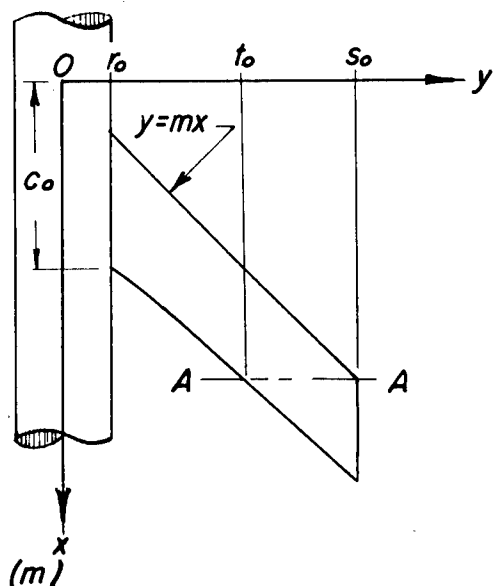
and since  $\Delta\phi$  at the leading edge is zero

$$\frac{L_w}{q} = \frac{2}{V_0} \int_{\text{span}} (\Delta\phi)_{T.E.} dy$$

where  $(\Delta\phi)_{T.E.}$  is the value of  $\Delta\phi$  on the trailing edge of the wing. Since  $(\Delta\phi)_{T.E.}$  also represents the total circulation about the wing chord, there results for the circulation  $\Gamma_w$  developed by the wing and the total wing lift  $L_w$

$$\Gamma_w = (\Delta\phi)_{T.E.}$$

$$L_w = \rho V_0 \int_{\text{span}} \Gamma_w dy \quad (51)$$



The equation for  $\Gamma_w$  can now be determined from equation (29). Between  $y = r_0$  and  $y = t_0$  (see sketch (m)) the value of  $\Gamma_w$  is a constant (this being the condition by which the shape of the trailing edge was determined). Between  $y = t_0$  and  $y = s_0$ ,  $\Gamma_w$  is given by the value of  $\Delta\phi$  along the section AA since there is no loading between this section and the trailing edge. Hence

$$\Gamma_w = 2V_0\alpha c_0 m \left[ 1 - \left( \frac{r_0}{mc_0} \right)^2 \right], \quad r_0 \leq y \leq t_0 \quad (52a)$$

and

$$\Gamma_w = 2V_0\alpha \left( \frac{s_0^2 - r_0^2}{s_0} \right) \left[ E(k_0, \psi_0) - k_0'^2 F(k_0, \psi_0) \right], \quad t_0 \leq y \leq s_0 \quad (52b)$$

where  $k_0$  and  $\psi_0$  are defined in the table of symbols.

Some care must be taken in order to find the span loading on the body. Since we are concerned here with the loading developed behind the wing-leading-edge fuselage juncture, it is necessary to subtract the value of  $\Delta\phi_b$  at this station, shown as station AA in sketch (n), from  $\Delta\phi_b$  at station BB also shown in sketch (n). For the total span loading, then, it will be necessary to add to this value the load accumulated on the nose of the body. Denote by  $(\Gamma_b)_0$  the increment of circulation developed by the nose of the body and by  $(\Gamma_b)_1$  the increment of circulation developed behind the wing-leading-edge fuselage juncture, that is, between stations AA and BB.<sup>7</sup> Hence,

---

<sup>7</sup>Slender wing theory gives zero loading behind station BB as long as the trailing vortex pattern does not vary.

$$\left. \begin{aligned} (\Gamma_b)_1 &= (\Delta\phi)_{T.E.} - (\Delta\phi)_{L.E.} \\ (\Gamma_b)_1 &= \rho_0 V_0 \int (\Gamma_b)_1 dy \end{aligned} \right\} \quad (53)$$

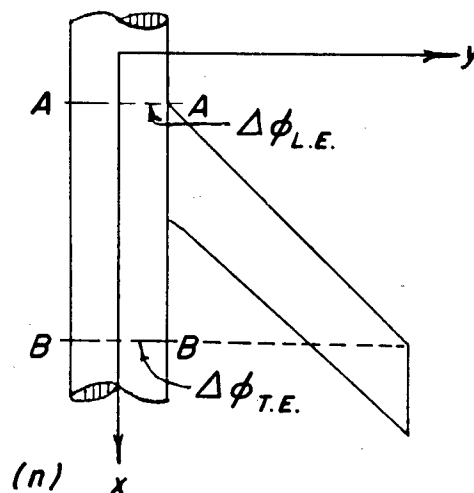
The value of  $(\Delta\phi)_{L.E.}$ , see sketch (n), can be obtained from equation (47) by setting  $t_1$  and  $s_1$  equal to  $r_1$ . By transformation of the result into the physical plane, one obtains

$$(\Delta\phi)_{L.E.} = 4V_0\alpha \sqrt{r_0^2 - y^2}$$

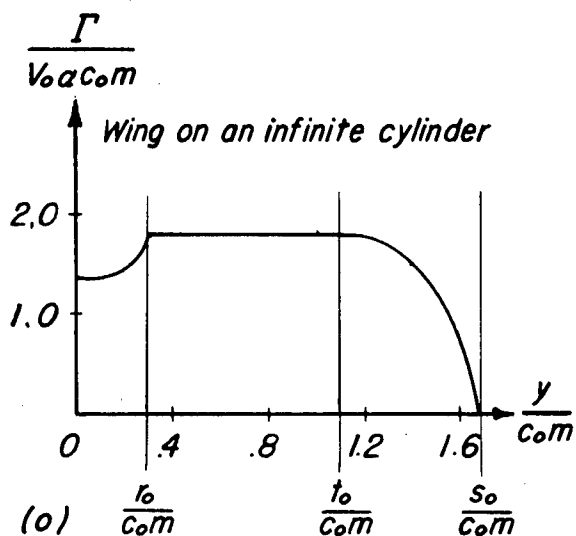
The span loading on the body is then given by

$$\begin{aligned} (\Gamma_b)_1 &= 2V_0\alpha \left\{ \frac{s_0^2 - r_0^2}{s_0} \left[ E_0 - E(k_0, \psi_2) + k_0'^2 F(k_0, \psi_2) - k_0'^2 K_0 \right] + \right. \\ &\quad \left. 2 \frac{t_0}{s_0} \sqrt{\frac{[(s_0^2 + r_0^2)^2 - 4s_0^2 y^2](r_0^2 - y^2)}{(t_0^2 + r_0^2)^2 - 4t_0^2 y^2}} - 2 \sqrt{r_0^2 - y^2} \right\} \quad (54) \end{aligned}$$

where  $k_0$  and  $\psi_2$  are given in the table of symbols.



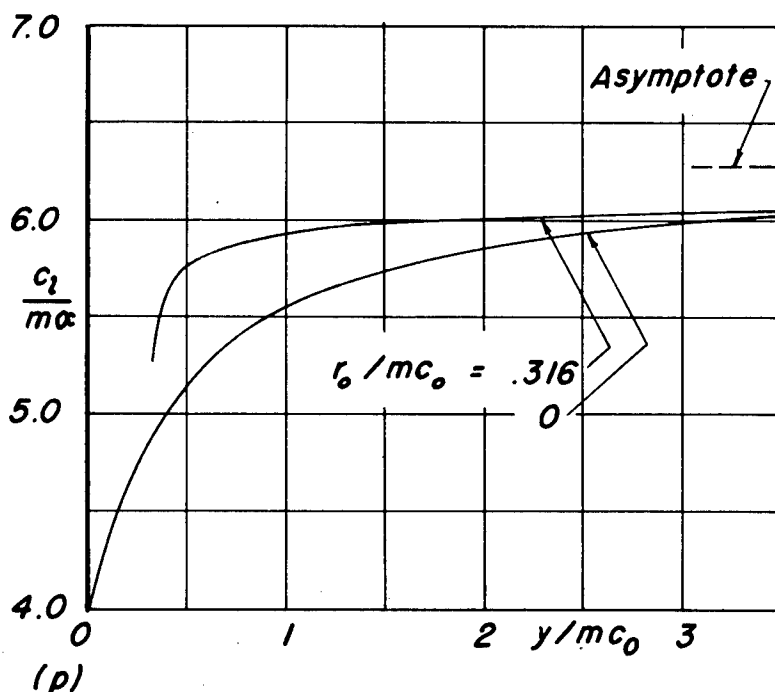




Sketch (o) shows the variation of the span loading over the wing and body for a body radius factor,  $r_o/mc_o$ , equal to 0.316 and a wing semispan factor,  $s_o/mc_o$  equal to 1.7.

Section lift.— The wing-section lift coefficient can be calculated readily by dividing the section chord into the value of the span loading at the same span station. Along sections not influenced by the tip cut-off this is especially simple since the span loading is constant. The value of the section lift curve follows immediately, therefore, from

table 2. Typical results are shown for a body radius factor equal to 0 and 0.316 in sketch (p).



Section drag.— The value of the section drag can be written

$$c_d = \alpha c_l + (c_d)_s \quad (55)$$

where  $(c_d)_s$  represents the suction force at the section leading edge. The magnitude of  $(c_d)_s$  can be evaluated (see, e.g., reference 8) by the equation

$$(c_d)_s = \frac{1}{qc} \frac{dF}{dy} \quad (56)$$

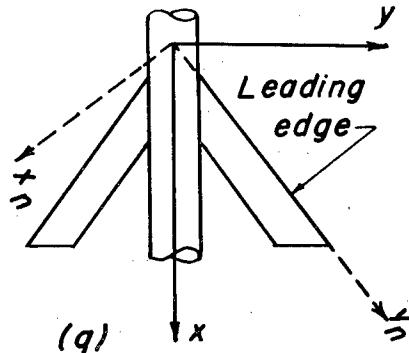
where  $dF/dy$  is the suction force in the free-stream direction per unit length normal to the free stream, and  $c$  is the local chord.

Define a new set of coordinates, as shown in sketch (q), such that  $y_n$  lies along and  $x_n$  lies perpendicular to the leading edge of one wing panel. Then if

$$G = \lim_{x_n \rightarrow 0} \beta_n \frac{u_n(x_n, y_n)}{V_0} \sqrt{x_n} \quad (57)$$

the suction-force component  $F$  (positive in the positive  $x_n$  direction) in the free-stream direction is given by the equation

$$\frac{dF}{dy} = - \frac{2\pi q}{\beta_n} G^2(x, y) \quad (58)$$



Now by differentiating equation (29) with respect to  $x$  and dividing by 2 (to convert  $\Delta u$  into  $u$ ), there results

$$u = mV_0\alpha \left( \frac{s^2 + r_0^2}{s^2} \right) \left[ E(k_0, \psi_0) - \frac{E_0}{K_0} F(k_0, \psi_0) + \frac{s^2(y^2 - r_0^2)}{yt(s^2 - r_0^2)} \sqrt{\frac{(y^2 - t^2)(y^2 t^2 - r_0^4)}{(s^2 - y^2)(s^2 y^2 - r_0^4)}} \right],$$

$$y/mc_0 \geq 1$$

and similarly  $v$  becomes

$$v = -V_0 \alpha \frac{y^2 + r_0^2}{y^2} \left( \frac{s}{t} \right) \sqrt{\frac{(y^2 t^2 - r_0^4)(t^2 - y^2)}{(s^2 y^2 - r_0^4)(s^2 - y^2)}}, \quad y/mc_0 \geq 1$$

Since the normal component  $u_n$  is given by the equation

$$u_n = \frac{mu - v}{\sqrt{1+m^2}}$$

there results

$$u_n = m^2 \frac{V_0 \alpha}{\sqrt{1+m^2}} \left( \frac{s^2 + r_0^2}{s^2} \right) \left[ E(k_0, \psi_0) - \frac{E_0}{K_0} F(k_0, \psi_0) \right] + \frac{V_0 \alpha}{yt \sqrt{1+m^2}} \sqrt{\frac{(y^2 - t^2)(y^2 t^2 - r_0^4)}{(s^2 - y^2)(s^2 y^2 - r_0^4)}} \\ \left[ \frac{m^2 (s^2 + r_0^2)(y^2 - r_0^2)}{s^2 - r_0^2} + \frac{s(y^2 + r_0^2)}{y} \right], \quad y/mc_0 \geq 1$$

By means of equation (57),  $G$  can now be calculated. Hence, since

$$\beta_n = 1/\sqrt{1+m^2},$$

$$G = \frac{\alpha(y^2 + r_0^2)}{yt(1+m^2)^{1/4}} \sqrt{\frac{(y^2 - t^2)(y^2 t^2 - r_0^4)}{2y(y^2 - r_0^2)}}$$

Finally, therefore, the suction force can be written

$$\frac{dF}{dy} = -2\pi q \frac{\alpha^2 (y^2 + r_0^2)}{y^2 t^2} \left[ \frac{(y^2 - t^2)(y^2 t^2 - r_0^4)}{2y(y^2 - r_0^2)} \right] \quad (59)$$

and, by using equations (55) and (56), the section drag coefficient can be written

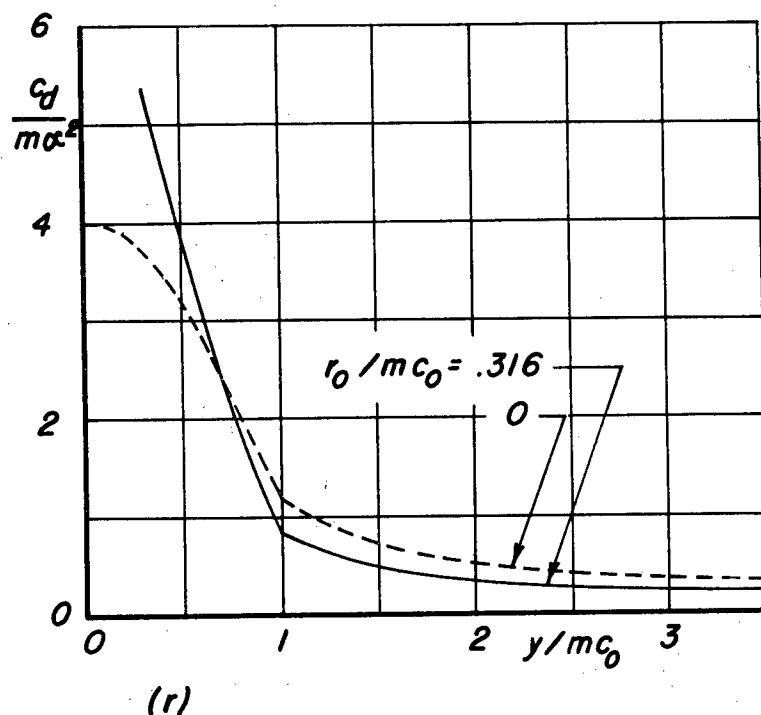
$$\frac{c_d}{\alpha^2 m} = \frac{c_l}{\alpha m} - \frac{\pi(y/mc_0)}{(c/c_0)} \frac{\left[1 + \left(\frac{r_0}{y}\right)^2\right] \left[1 - \left(\frac{t}{y}\right)^2\right] \left[1 - \left(\frac{r_0}{y}\right)^2 \left(\frac{r_0}{t}\right)^2\right]}{1 - \left(\frac{r_0}{y}\right)^2}, \quad y/mc_0 \geq 1$$

(60a)

In the region where the leading-edge suction force cannot be affected by the trailing-edge shape, equation (60) reduces to the simpler form

$$\frac{c_d}{\alpha^2 m} = \frac{c_l}{\alpha m} - \frac{\pi(y/mc_0)}{(c/c_0)} \left[1 - \left(\frac{r_0}{y}\right)^4\right], \quad r_0/mc_0 \leq y/mc_0 \leq 1 \quad (60b)$$

The variation of the section drag coefficient is shown in sketch (r) for two wings: one without a body, and the other with a body radius factor equal to 0.316.



Total lift.— The lift on the wing, the body, and the combination can now be evaluated by means of equations (51) and (53) since the expressions for  $\Gamma$  are given by equations (52) and (54). The integration required is somewhat involved algebraically, but the final result can again be expressed in terms of elliptic integrals. Thus, defining  $\Lambda_O(k, \psi)$  by

$$\Lambda_O(k, \psi) = \frac{2}{\pi} \left[ KE'(k, \psi) + EF'(k, \psi) - KF'(k, \psi) \right] \quad (61)$$

(tabular values for  $\Lambda_O$  can be found in reference 9), the total lift carried by the wing is

$$\begin{aligned} \frac{L_W}{q\alpha} = 2 \frac{s_0^2 - r_0^2}{s_0} \left\{ \frac{t_0^2 + r_0^2}{t_0} \left[ E_{2-k_0'^2} K_2 \right] - 4r_0 \left[ E_{0-k_0'^2} K_0 \right] \right\} - \\ \pi \left[ \left( \frac{s_0^2 + r_0^2}{s_0} \right)^2 - \left( \frac{t_0^2 - r_0^2}{t_0} \right)^2 \right] \Lambda_O(k_2, \psi_4) + 2\pi \left[ \left( \frac{s_0^2 + r_0^2}{s_0} \right)^2 - \left( \frac{t_0^4 + r_0^4}{t_0^2} \right) \right] \end{aligned} \quad (62)$$

Equation (62) agrees with the results presented in references 3 and 4 when  $t_0 = r_0$  (the case of a triangular wing on a body) and  $r_0 = 0$  (the case of no body), respectively. When  $s_0$  equals  $t_0$ , that is, when there is no wing,  $L_W$  equals 0.

The lift on the body will be computed in two parts just as was the span loading on the wing: the lift on the portion of the body behind the wing-leading-edge fuselage juncture  $(L_b)_1$ , and the lift on the nose of the body  $(L_b)_0$ . It is a well-known result of Munk's airship theory that the lift on the pointed nose is just

$$\frac{(L_b)_0}{q\alpha} = 2\pi r_0^2 \quad (63)$$

and is independent of the shape of the nose.<sup>8</sup> The value of the lift in the vicinity of the wing follows from the integration of equation (54) according to equation (53). The total lift on the body can then be written

---

<sup>8</sup>In this report, it is assumed that the nose is always ahead of the wing, that is, the portion of the body on which the wing is mounted is everywhere a circular cylinder.

---

$$\frac{L_b}{q\alpha} = \frac{(L_b)_0 + (L_b)_1}{q\alpha} = .2 \frac{s_0^2 - r_0^2}{s_0} \left[ 4r_0 \left( E_0 - k_0'^2 K_0 \right) - \frac{t_0^2 + r_0^2}{t_0} \left( E_2 - k_0'^2 K_2 \right) \right] +$$

$$\pi \left[ \left( \frac{s_0^2 + r_0^2}{s_0} \right)^2 - \left( \frac{t_0^2 - r_0^2}{t_0} \right)^2 \right] \Lambda_0(k_2, \psi_4) - 2\pi r_0^2 \quad (64)$$

Setting  $t_0 = r_0$ , one finds the result given in reference 3 for a triangular wing mounted on the cylindrical portion of a pointed body.

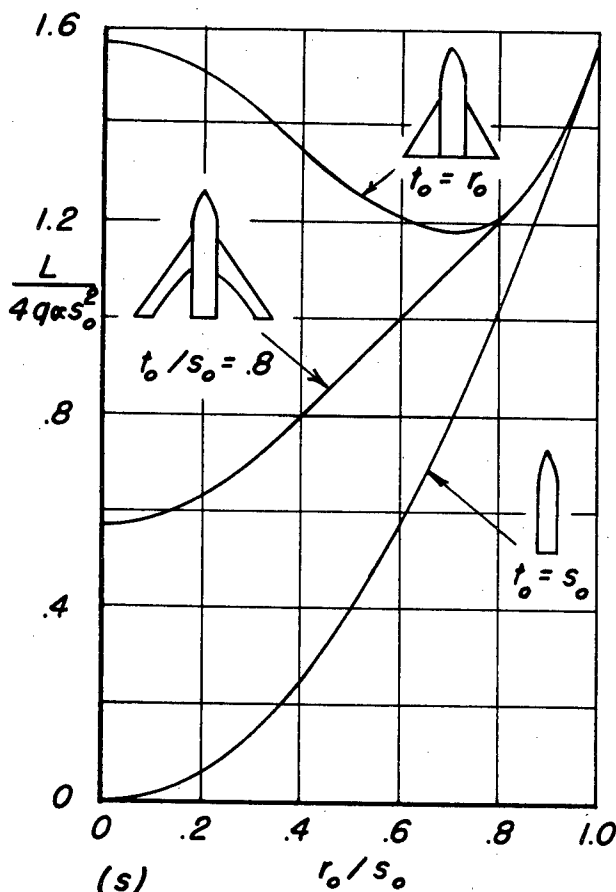
If  $t_0 = r_0 = s_0$ , the wing disappears and equation (64) reduces<sup>9</sup> to equation (63). If  $r_0 = 0$ ,  $L_b$  reduces to zero.

Finally, the sum of equations (62) and (64) gives for the total lift of the wing-body combination, including the nose of the body,

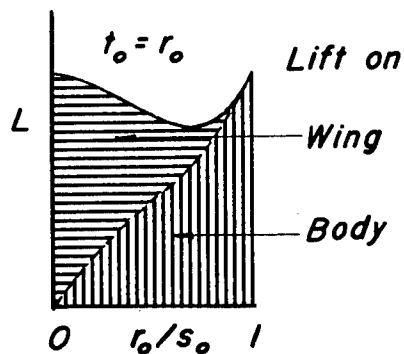
$$\frac{L}{q\alpha} = 2\pi \left( \frac{s_0^4 + r_0^4}{s_0^2} - \frac{t_0^4 + r_0^4}{t_0^2} + r_0^2 \right) \quad (65)$$

Sketches (s) and (t) show the total lift on various wing-body combinations together with its division into the component parts carried separately by the wing and body. Various lift coefficients, depending on the choice of the reference area, can be formulated by means of the area-span relationship given in figure 1.

Total drag.- In general, the vortex drag can be calculated by finding the momentum transport through a plane perpendicular to the  $x$  axis and located infinitely far behind the airplane. In slender wing theory the calculation of the total drag is simplified in two



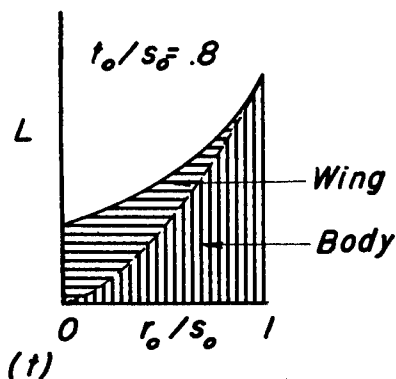
<sup>9</sup>Note that  $\Lambda_0(k, 1) = 1$ .



ways: first, the vortex drag becomes the total drag (neglecting, of course, viscosity), and second, in the calculation of this drag the reference plane can be located immediately behind the airplane since the flow there is the same as it is infinitely far back.

Hence, a momentum balance gives for the drag

$$D = -\rho_0 \int_{r_0}^{s_0} w_0 \Delta\phi dy + \rho_0 r_0 \int_0^\pi (v_r)_{r=r_0}(\phi)_{r=r_0} d\theta \quad (66a)$$



where  $w$  is the value of the vertical induced velocity behind the wing in the  $z = 0$  plane. It is more convenient to perform this integration in the  $\xi_1$  plane. Equation (66a) can be put in the form

$$D = -\frac{\rho_0}{2} \int_{r_1}^{s_1} \left(1 + \frac{y_1}{\sqrt{y_1^2 - r_1^2}}\right) w \Delta\phi_1 dy_1 - \rho_0 \int_0^{r_1} w \Delta\phi_1 dy_1 \quad (66b)$$

where  $w$  and  $\Delta\phi_1$  are given in the following.

For  $r_1^2 \leq y_1^2 \leq t_1^2$ , that is, between the body and the trailing edge, it is seen from equations (39b) and (31) that

$$\left. \begin{aligned} w &= -V_0 \alpha \left[ 1 - 2y_1 \frac{y_1 - \sqrt{y_1^2 - r_1^2}}{r_1^2} \right] \sqrt{\frac{t_1^2 - y_1^2}{s_1^2 - y_1^2}} \\ \Delta\phi_1 &= 2V_0 \alpha \sqrt{s_1^2 - r_1^2} (E_1 - k_1'^2 K_1) \end{aligned} \right\} \quad (67a)$$

For  $t_1^2 \leq y_1^2 \leq s_1^2$ , that is, on the wing, it is seen from equations (39a) and (29) that

$$\left. \begin{aligned} w &= -V_0 \alpha \\ \Delta \phi_1 &= 2V_0 \alpha \sqrt{s_1^2 - r_1^2} \left[ E(k_1, \psi_1) - k_1'^2 F(k_1, \psi_1) \right] \end{aligned} \right\} \quad (67b)$$

Finally, for  $y_1^2 \leq r_1^2$ , that is, on the body, equations (38a) and (47) give

$$\left. \begin{aligned} w &= -V_0 \alpha \\ \Delta \phi_1 &= 2V_0 \alpha \sqrt{s_1^2 - r_1^2} \left[ E_1 - E(k_1, \psi_3) + k_1'^2 F(k_1, \psi_3) - \right. \\ &\quad \left. k_1'^2 K_1 \right] + 2V_0 \alpha \sqrt{\frac{(s_1^2 - y_1^2)(r_1^2 - y_1^2)}{t_1^2 - y_1^2}} \end{aligned} \right\} \quad (67c)$$

The substitution of equations (67a), (67b), and (67c) into equation (66b) yields after integration

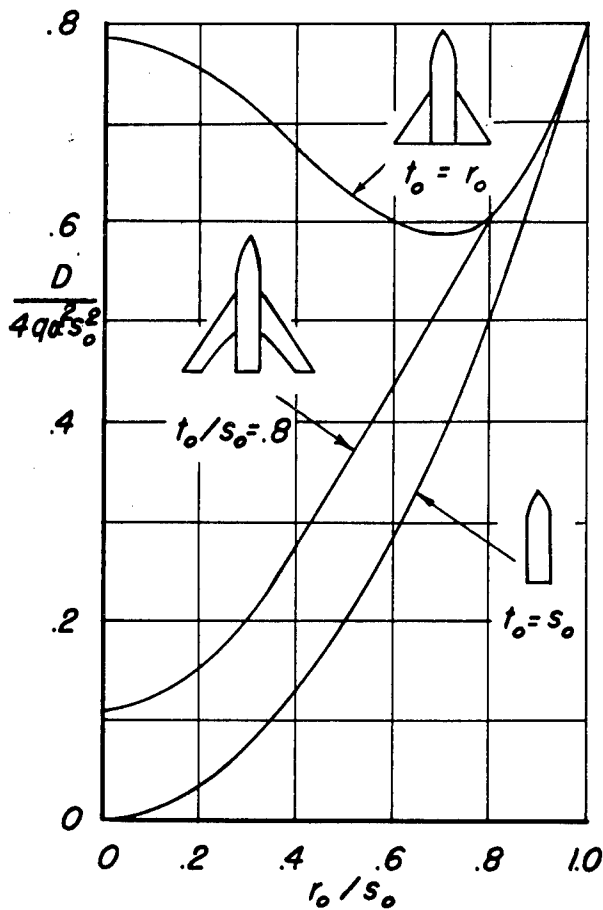
$$\frac{D}{q\alpha^2} = \frac{L}{2q\alpha} - 4(s_1^2 - r_1^2)(E_1 - k_1'^2 K_1)(E_1' - k_1'^2 K_1') \quad (68)$$

where  $L/q\alpha$  is given in equation (65). In the  $\xi$  plane equation (68) can be written in the dimensionless form

$$\frac{D}{4q\alpha^2 s_0^2} = \frac{L}{8q\alpha s_0^2} - \left( \frac{s_0^2 - r_0^2}{s_0^2} \right)^2 (E_0 - k_0'^2 K_0)(E_0' - k_0'^2 K_0') \quad (69)$$

which for  $r_0 = 0$  agrees with the results of reference 4. Equation (69) also checks with the result obtained for the drag by the method, presented in the preceding section on section drag, based on the calculation of the suction force along the wing leading edge.





(u)

Sketch (u) shows the total drag on various wing-body combinations.

Chord loading.- In order to find the center of pressure and pitching moment, it is convenient to find first the chord loading, which we will define as the value of  $\int (\Delta p / q\alpha) dy$  where the integration is carried over the wing and body. The chord loading can also be obtained by evaluating the expression  $d(L/q\alpha)/dx$  since the latter term is equal to  $\int (\Delta p / q\alpha) dy$ . As a check, both methods were used to derive the following expressions.

For the part of the chord loading contributed by the wing it can be shown that

$$2 \int_{t_o}^{s_o} \left( \frac{\Delta p}{q\alpha} \right)_w dy = \frac{d}{dx} \left( \frac{L_w}{q\alpha} \right) =$$

$$\frac{4(s_o^4 - r_o^4)}{s_o^3} m \left( \pi - \arcsin \frac{2s_o r_o}{s_o^2 + r_o^2} \right), \quad r_o/m \leq x \leq c_o \quad (70a)$$

$$2 \int_{t_0}^{s_0} \left( \frac{\Delta p}{q\alpha} \right)_w dy = \frac{d}{dx} \left( \frac{L_w}{q\alpha} \right) = \frac{4(s_0^4 - r_0^4)}{s_0^3} m$$

$$\left\{ \left( 1 - \frac{E_0}{K_0} \right) \pi \left[ 1 - \frac{\Lambda_0(k_2, \psi_4)}{2} \right] + \frac{s_0}{t_0} \left( \frac{t_0^2 + r_0^2}{s_0^2 - r_0^2} \right) \left( E_2 - \frac{E_0}{K_0} K_2 \right) \right\}, c_0 \leq x \quad (70b)$$

For the part contributed by the body behind the leading-edge fuselage juncture it can be shown that

$$2 \int_0^{r_0} \left( \frac{\Delta p}{q\alpha} \right)_b dy = \frac{d}{dx} \frac{(L_b)_1}{q\alpha} = \frac{4(s_0^4 - r_0^4)}{s_0^3} m \arcsin \frac{2s_0 r_0}{s_0^2 + r_0^2}, r_0/m \leq x \leq c_0 \quad (71a)$$

$$2 \int_0^{r_0} \left( \frac{\Delta p}{q\alpha} \right)_b dy = \frac{d}{dx} \frac{(L_b)_1}{q\alpha} = \frac{4(s_0^4 - r_0^4)}{s_0^3} m$$

$$\left[ \left( 1 - \frac{E_0}{K_0} \right) \frac{\pi}{2} \Lambda_0(k_2, \psi_4) + \frac{s_0}{t_0} \left( \frac{t_0^2 + r_0^2}{s_0^2 - r_0^2} \right) \left( K_2 \frac{E_0}{K_0} - E_2 \right) \right] \quad (71b)$$

The total chord loading can be obtained by combining equations (70) and (71). There results the expressions

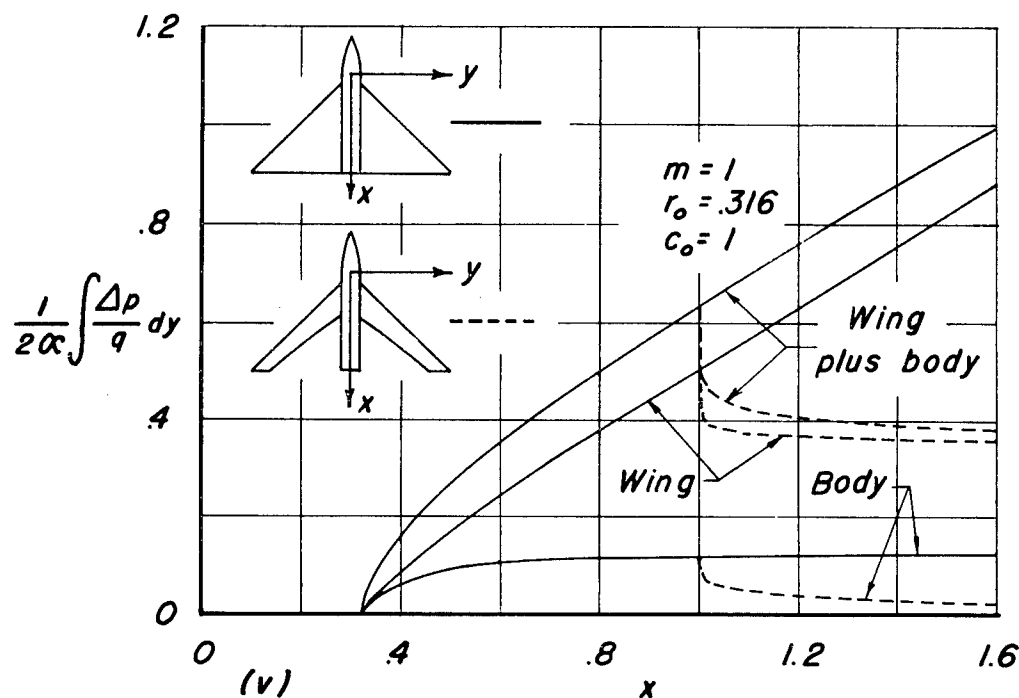
for  $r_0/m \leq x \leq c_0$

$$\frac{d}{dx} \left( \frac{L}{q\alpha} \right) = 4\pi m \left( \frac{s_0^4 - r_0^4}{s_0^3} \right) \quad (72a)$$

and for  $c_0 \leq x$

$$\frac{d}{dx} \left( \frac{L}{q\alpha} \right) = 4\pi m \left( \frac{s_0^4 - r_0^4}{s_0^3} \right) \left( 1 - \frac{E_0}{K_0} \right) \quad (72b)$$

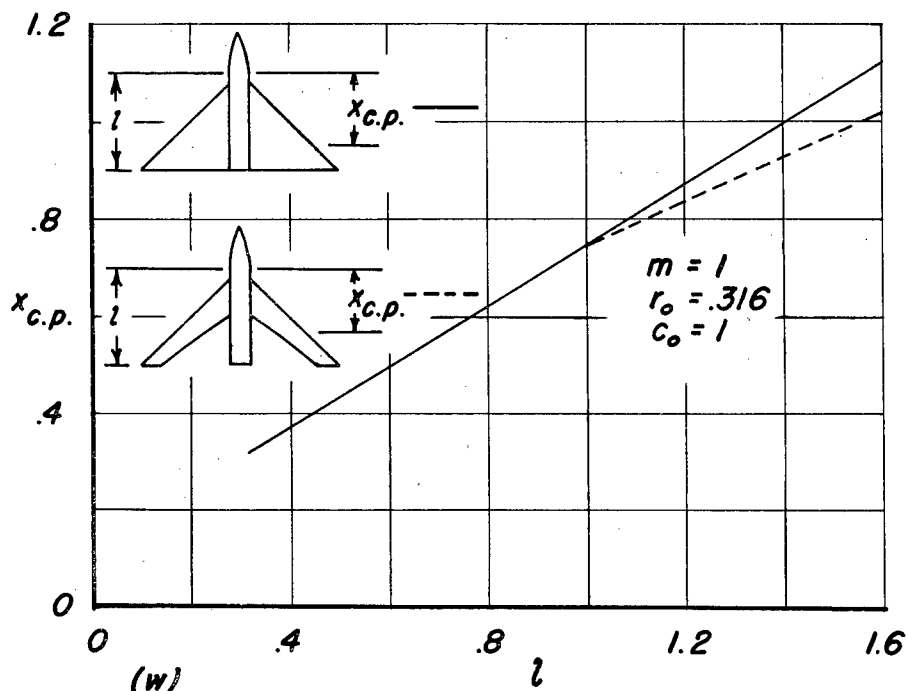
Sketch (v) shows the variation of the chord loading with  $x$  for  $r_o/mc_o$  equal to 0.316.



Center of pressure.— The results of the last section can be used to determine the center of pressure  $x_{c.p.}$ . The value of  $x_{c.p.}$  is given by the equation

$$x_{c.p.} = \frac{\int_{r_o/m}^{s_o/m} x \frac{dL}{dx} dx}{L} \quad (73)$$

which excludes the loading on the nose. By means of equation (73) sketch (w) was constructed.



## II - ADDITION OF A HORIZONTAL TAIL

It is possible to use the calculations given in the first part of this report to find the forces and moments induced on a horizontal tail by the presence of the wing and body. The same assumptions that were used for the solution of the load distribution over the wing and body will be made here. Hence, the results will be principally valid for airplanes having highly swept wings and tails or flying at Mach numbers approaching 1.

In addition to the basic assumptions by which slender wing theory is defined, however, some additional assumptions must be made concerning the behavior of the vortex sheet trailing behind the wing and passing by the tail. Actually these trailing vortices provide the only means by which the wings can signal their presence to the tail, and except for them the slender wing theory analysis of the tail effectiveness would be identical to that described in part I for the wing. Only two types of trailing vortex patterns will be investigated. One composed of a flat vortex sheet situated entirely in the  $z = 0$  plane (the plane of the wing), and the other composed of two completely rolled up point vortices

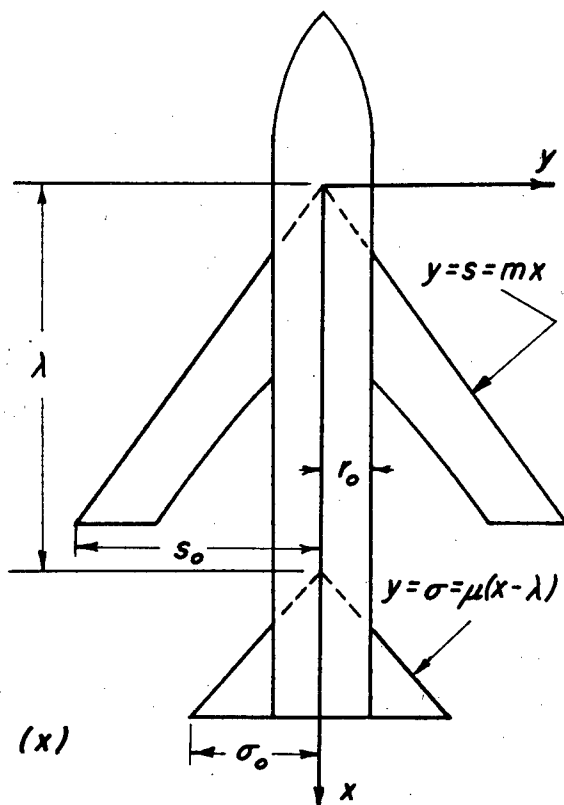
situated symmetrically with respect to the  $y = 0$  plane, located a distance  $h$  above the  $z = 0$  plane and a distance  $a$  from plane of symmetry. These patterns represent the two extremes of the actual physical behavior of a trailing vortex wake. It is to be expected that the sheet is more representative of the true wake when the tail is located only a short distance behind the wing. On the other hand, the two point vortices should be valid for tails located a large distance behind the wing. An indication of the magnitude of the distances at which the two assumptions are accurate can be obtained in reference 10.

### Method of Solution and Boundary Conditions

The partial differential equation that governs the flow in the vicinity of the tail is, of course, identical to the one studied in the first part of this report, namely, Laplace's equation applied to a  $yz$  plane (equation (2)). In fact, the general discussion of boundary conditions and forms of solution given in part I still applies here. Hence, the Joukowski transformation can again be used, the  $\xi$  plane having the same relation to the  $\xi_1$  plane as before and the integral relationship given as equation (15) still applying.

The only mathematical difference between the study of the wing and tail can be seen at once in the application of equation (15). In the case of a flat wing, the vertical induced velocity  $w$  in equation (15) was known to be a constant over the region occupied by the wing plan form. In the case of a flat horizontal tail, on the other hand, the value of  $w$  over the region occupied by the tail plan form is composed of two parts: one, the constant value fixed by the inclination of the surface to the free stream, and the other, a distribution that is just equal and opposite to the vertical velocity induced over the region by the vortices trailing from the wing. Effectively, therefore, the analysis of a horizontal tail is the same as that for a wing with a given variation of twist and camber.

The additional notation necessary for the description of the pertinent tail parameters is shown in sketch (x). The distance from the  $x$  axis to the tail leading edge is represented by  $\sigma$ , and the slope of the tail leading edge is designated by  $\mu$ . In this report, only triangular tail shapes will be considered; however, more complicated shapes could be analyzed by the method presented.



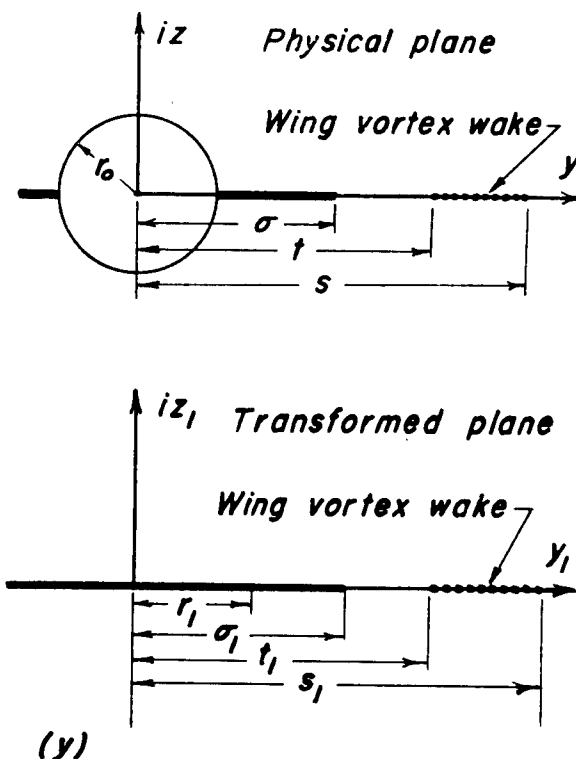
### Solution for Trailing Vortex Sheet

Since the vortex sheet from the wing is assumed to lie entirely in the  $z_1 = 0$  plane, and since the outer extremities of this sheet are at  $\pm s_1$  (see sketch (y)), the study of this case can commence with the inversion of the integral equation (15) of part I.

$$w_1(y_1) = -\frac{1}{2\pi} \int_{-s_1}^{s_1} \frac{\Delta v_1(y_2)}{y_1 - y_2} dy_2 \quad (74)$$

For  $t_1^2 < y_1^2 < s_1^2$ , the value of  $\Delta v_1(y_2)$  is given by equation (25a) and for  $\sigma_1^2 < y_1^2 < t_1^2$ ,

$$\Delta v_1(y_2) = 0 \quad (75)$$



Substitute these two values of  $\Delta v_1$  into equation (74) and apply the boundary condition that  $w_1$  equals  $-V_0\alpha$  in the interval  $0 < y_1^2 < \sigma_1^2$ . Then, assuming  $t_1^2 > \sigma_1^2$ , that is, the vortex sheet from the wing does not cross the tail<sup>10</sup> (the condition shown in sketch (y)), there is obtained, after inversion (see appendix B) and some manipulation, the value of  $\Delta v_1$  on the tail. Thus

for  $0 < y_1^2 < \sigma_1^2$  and for  $t_1^2 > \sigma_1^2$

$$\Delta v_1(y_1) = -\frac{2V_0\alpha y_1}{\sqrt{\sigma_1^2 - y_1^2}} - \frac{2V_0\alpha y_1}{\pi\sqrt{\sigma_1^2 - y_1^2}} \int_{t_1^2}^{s_1^2} \frac{d\eta}{y_1^2 - \eta} \sqrt{\frac{(\eta - t_1^2)(\eta - \sigma_1^2)}{(s_1^2 - \eta)(\eta - r_1^2)}} \quad (76)$$

This solution for  $\Delta v_1$  can now be used to determine the aerodynamic characteristics of the tail in the presence of the vortex sheet trailing back from the wing.

<sup>10</sup>This assumption applies to all subsequent analysis of the tail and vortex sheet combinations.

Span loading.— The spanwise variation of circulation generated by the tail surface is given by the expression

$$\Delta\phi_t = \int_{\sigma}^y \Delta v(y_2) dy_2 \quad (77)$$

where  $\Delta v$  is given in the  $\xi_1$  plane by equation (76). On the portion of the  $\xi_1$  plane that is covered by the tail surface (i.e., for  $r_1^2 < y_1^2 < \sigma_1^2$ ) this yields

$$\Delta\phi_{1t} = 2V_0\alpha \sqrt{\sigma_1^2 - y_1^2} - \frac{2V_0\alpha}{\pi} \int_{t_1^2}^{s_1^2} \sqrt{\frac{\eta - t_1^2}{(s_1^2 - \eta)(\eta - r_1^2)}} \arctan \sqrt{\frac{\sigma_1^2 - y_1^2}{\eta - \sigma_1^2}} d\eta \quad (78)$$

To determine the span loading on the body it is necessary to subtract the value of  $\Delta\phi_{1t}$  at the tail-leading-edge fuselage juncture. This value is obtained from equation (78) by placing  $\sigma_1 = r_1$ . The span loading on the body (i.e., for  $0 < y_1^2 < r_1^2$ ) is then given by the formula

$$\begin{aligned} \Delta\phi_{1t} = & 2V_0\alpha \left( \sqrt{\sigma_1^2 - y_1^2} - \sqrt{r_1^2 - y_1^2} \right) + \\ & \frac{2V_0\alpha}{\pi} \int_{t_1^2}^{s_1^2} \sqrt{\frac{\eta - t_1^2}{(s_1^2 - \eta)(\eta - r_1^2)}} \arctan \sqrt{\frac{r_1^2 - y_1^2}{\eta - r_1^2}} d\eta - \\ & \frac{2V_0\alpha}{\pi} \int_{t_1^2}^{s_1^2} \sqrt{\frac{\eta - t_1^2}{(s_1^2 - \eta)(\eta - r_1^2)}} \arctan \sqrt{\frac{\sigma_1^2 - y_1^2}{\eta - \sigma_1^2}} d\eta \quad (79) \end{aligned}$$

Equations (78) and (79) have been transformed to the  $\xi$  plane and the results are shown in figure 2(a). In this and in all following numerical examples the wing will be fixed as the special type studied in part I having the measures  $s_0/mc_0 = 1.7$ ,  $t_0/mc_0 = 1.091$  and  $r_0/mc_0 = 0.316$ .



Chordwise load distribution on the tail.— The distribution of load over the tail surface can be calculated from the equation

$$\left(\frac{\Delta p}{q\alpha}\right)_t = \frac{2}{V_0\alpha} \frac{\partial \Delta \phi_t}{\partial x} = \frac{2}{V_0\alpha} \frac{\partial \Delta \phi_{1t}}{\partial \sigma_1} \frac{d\sigma_1}{dx} \quad (80)$$

where the value of  $\partial \Delta \phi_{1t} / \partial \sigma_1$ , determined from equation (78), is given by the expression

$$\frac{\partial \Delta \phi_{1t}}{\partial \sigma_1} = \frac{2V_0\alpha\sigma_1}{\sqrt{\sigma_1^2 - y_1^2}} + \frac{2V_0\alpha\sigma_1}{\pi \sqrt{\sigma_1^2 - y_1^2}} \int_{t_1^2}^{s_1^2} \frac{(\eta - t_1^2) d\eta}{\sqrt{(s_1^2 - \eta)(\eta - r_1^2)(\eta - \sigma_1^2)(\eta - t_1^2)}} \quad (81)$$

By means of the substitutions

$$k_4^2 = \frac{(\sigma_1^2 - r_1^2)(s_1^2 - t_1^2)}{(s_1^2 - \sigma_1^2)(t_1^2 - r_1^2)}, \quad \text{sn}^2 u = \frac{(s_1^2 - \sigma_1^2)(\eta - t_1^2)}{(s_1^2 - t_1^2)(\eta - \sigma_1^2)} \quad (82)$$

equation (81) can be reduced to

$$\frac{\partial \Delta \phi_{1t}}{\partial \sigma_1} = - \frac{2V_0\alpha\sigma_1 \Lambda_0(k_5, \psi_9)}{\pi \sqrt{\sigma_1^2 - y_1^2}} \quad (83)$$

where

$$\psi_9 = \sqrt{\frac{t_1^2 - r_1^2}{s_1^2 - r_1^2}} \quad (84)$$

Hence, the loading on the tail can be written in the closed form

$$\left(\frac{\Delta p}{q\alpha}\right)_t = \frac{4\sigma_1 \Lambda_0(k_5, \psi_9)}{\sqrt{\sigma_1^2 - y_1^2}} \frac{d\sigma_1}{dx} \quad (85)$$

and since

$$\frac{d\sigma_1}{dx} = \frac{\sigma^2 - r_0^2}{\sigma^2} \mu$$

the final expression obtained by transforming equation (85) to the  $\xi$  plane is

$$\left(\frac{\Delta p}{q\alpha}\right)_t = \frac{4(\sigma^4 - r_0^4)\mu}{\sigma^3} \Lambda_0(k_4, \psi_8) \quad (86)$$

where  $k_4$  and  $\psi_8$  are the transformed values of  $k_5$  and  $\psi_9$  and are given in the table of symbols.

Total lift on the tail.— The total lift on the tail can be evaluated by use of the equation

$$\frac{L_t}{q\alpha} = - \frac{2}{V_0\alpha} \int_0^\sigma \Delta\Phi(y) dy \quad (87)$$

which becomes in the  $\xi_1$  plane,

$$\frac{L_t}{2q\alpha} = \frac{1}{V_0\alpha} \int_0^{\sigma_1} \Delta\Phi_1(y_1) dy_1 + \frac{1}{V_0\alpha} \int_{r_1}^{\sigma_1} \frac{y_1 \Delta\Phi_1(y_1) dy_1}{\sqrt{y_1^2 - r_1^2}} \quad (88)$$

The value of  $\Delta\Phi_1$  is given by the equations (78) and (79). Substitute these expressions into equation (88) and, after integration, there results

$$\begin{aligned} \frac{L_t}{2q\alpha} = & \pi(t_1^2 - r_1^2 - s_1^2 + \sigma_1^2) \Lambda_0(k_5, \psi_9) + \\ & 2 \sqrt{(s_1^2 - \sigma_1^2)(t_1^2 - r_1^2)} \left[ E_5 - \left( \frac{t_1^2 - \sigma_1^2}{s_1^2 - \sigma_1^2} \right) K_5 \right] \end{aligned} \quad (89)$$

In the  $\xi$  plane this can be written

$$\begin{aligned} \frac{L_t}{2q\alpha} = & - \pi \left[ \frac{(s_0^2 - t_0^2)(s_0^2 t_0^2 - r_0^4)}{s_0^2 t_0^2} - \frac{(\sigma_0^2 - r_0^2)^2}{\sigma_0^2} \right] \Lambda_0(k_4, \psi_8) + \\ & \frac{2(t_0^2 - r_0^2)}{t_0 s_0} \sqrt{(s_0^2 - \sigma_0^2)(s_0^2 \sigma_0^2 - r_0^4)} \left( E_4 - \frac{k_4'^2}{k_0'^2} K_4 \right) \end{aligned} \quad (90)$$

A plot of this equation is shown in figure 3(a) for  $r_0/mc_0 = 0.316$ .

Drag.- The drag of the tail can be calculated from the equation

$$D_t = \alpha L_t + F_t \quad (91)$$

where  $L_t$  is given by equation (90) and  $F_t$  is the suction force at the leading edge. In a manner similar to that given in the first part of this report under the subheading "Section drag," this force is obtained from the equation

$$F_t = - \frac{2\pi q}{\beta_n} \int_{r_0}^{\sigma} G^2 dy \quad (92)$$

As before

$$G = \lim_{x_n \rightarrow 0} \beta_n \frac{u_n(x_n, y_n)}{V_0} \sqrt{x_n} \quad (93)$$

the values of  $u_n$  and  $x_n$  being, respectively, the normal velocity to and the normal distance from the leading edge. Substituting these values into equation (93) gives

$$G^2 = \frac{\alpha^2}{2\sqrt{1+\mu^2}} \left( \frac{y^4 - r_0^4}{y^3} \right) \Lambda_0^2(k_4, \psi_B) \quad (94)$$

and the expression for the suction force can be written

$$F_t = - V_0^2 \alpha^2 \rho \pi \int_{r_0}^{\sigma} \left( \frac{y^4 - r_0^4}{y^3} \right) \Lambda_0^2(k_4, \psi_B) dy \quad (95)$$

Hence, the total drag becomes

$$\frac{D_t}{\alpha^2 q} = \frac{L_t}{\alpha q} - 2\pi \int_{r_0}^{\sigma} \left( \frac{\sigma^4 - r_0^4}{\sigma^3} \right) \Lambda_0^2(k_4, \psi_B) dy \quad (96)$$

This equation is plotted in figure 4(a) for  $r_0/mc_0 = 0.316$ .

Chord loading.- A closed formula for the loading can be obtained by carrying out the integration  $\int (\Delta p/q\alpha)_t dy$  over the tail or by evaluating  $d(L_t/q\alpha)/dx$ . However, since the term  $\Lambda_0(k_4, \psi_B)$  in the expression for  $\Delta p/q\alpha$  does not involve  $y$ , it is easier to evaluate  $\int (\Delta p/q\alpha)_t dy$ . Thus, using equation (85), the chord loading in the  $\xi_1$  plane is given by

$$\begin{aligned}
 2 \int_0^{\sigma} \left( \frac{\Delta p}{q\alpha} \right)_t dy &= \int_0^{\sigma_1} \left( \frac{\Delta p}{q\alpha} \right)_t dy_1 + \int_{r_1}^{\sigma_1} \frac{y_1 \left( \frac{\Delta p}{q\alpha} \right)_t dy_1}{\sqrt{y_1^2 - r_1^2}} \\
 &= 4\pi\sigma_1 \Lambda_0(k_5, \psi_8) \frac{d\sigma_1}{dx}
 \end{aligned} \tag{97a}$$

In the  $\xi$  plane this becomes

$$2 \int_0^{\sigma} \left( \frac{\Delta p}{q\alpha} \right)_t dy = 4\pi\mu \left( \frac{\sigma^4 - r_0^4}{\sigma^3} \right) \Lambda_0(k_4, \psi_8) \tag{97b}$$

(This checks with the result found by differentiating  $L_t/q\alpha$  with respect to  $x$ ).

Center of pressure.— The center of pressure can be calculated by means of the formula

$$x_{c.p.} = \frac{\int_{r_0/\mu}^{\sigma_0/\mu} x \frac{dL_t}{dx} dx}{L_t} \tag{98}$$

where  $dL_t/dx$  is the result just obtained in the previous section and  $L_t$  is given by equation (90). Placing these values into equation (98) yields

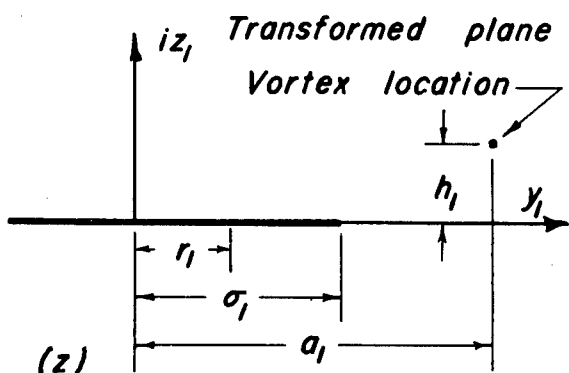
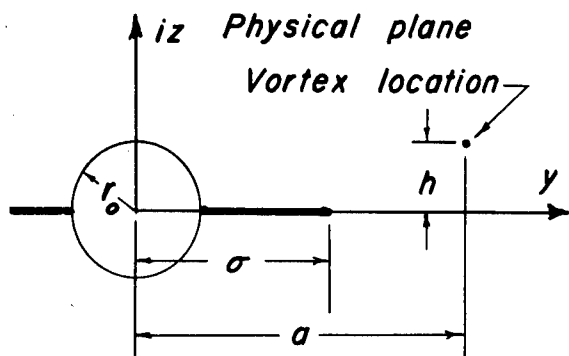
$$x_{c.p.} = \frac{4\pi q\alpha}{L} \int_{r_0}^{\sigma_0} \left( \frac{\sigma^4 - r_0^4}{\sigma^2} \right) \Lambda_0(k_4, \psi_8) dx \tag{99}$$

A graph of this result is shown in figure 5(a) for  $r_0/mc_0 = 0.316$ .

#### Solution for Rolled Up Vortices

As was pointed out in the preceding section where the method of solution was discussed, the manner in which the present problem will be attacked is as follows: First, the velocities induced at the surface of the wing and body by two point vortices located somewhere in space will be calculated; second, a solution will be formulated (by methods identical to those used in part I of this report) that will just cancel the vortex induced velocity component normal to the surface of the wing or body; third, an additional solution will be formulated that will fit the boundary conditions prescribed for the tail surface (in this report only a flat-plate tail surface will be considered).

As usual, it is simpler to work with the transformed  $\xi_1$  plane than with the physical  $\xi$  plane. Hence, again the Joukowski transformation will be applied to the field equation and boundary conditions at the outset of the problem. See sketch (z).



The velocity potential at a point  $(y_1, z_1)$  in the  $\xi_1$  plane induced by a pair of point vortices located at  $y_1 = \pm a_1$  and  $z_1 = h_1$  is given by the equation

$$\phi_v = \frac{\Gamma_w}{2\pi} \int_{-a_1}^{a_1} \frac{(z_1 - h_1) dy_2}{(y_1 - y_2)^2 + (z_1 - h_1)^2} \quad (100)$$

where  $\Gamma_w$  is the strength of the circulation carried by the wing panels and trailing back from the wing tips. The value of  $\Gamma_w/V_0 \alpha mc_0$  that corresponds to the swept-back wings studied in part I of this report is given by equation (32a), thus

$$\frac{\Gamma_w}{V_0 \alpha mc_0} = 2 \left[ 1 - \left( \frac{r_0}{mc_0} \right)^2 \right]$$

The values of  $a_1$  and  $h_1$  depend, of course, on the span of the wing. In order to compare the following results for the rolled up vortices with those obtained for the sheet vortices in the preceding section, the numerical results presented in the succeeding examples will be for  $s_0/mc_0 = 1.7$ ,  $t_0/mc_0 = 1.091$ , and  $r_0/mc_0 = 0.316$ . This particular choice of parameters fixes the span-loading curve for the wing to be that shown in sketch (o). A reasonable choice for the value of  $a$  can be calculated by replacing the figure in sketch (o) bounded by the lines  $y = r_0$ ,  $\Gamma = 0$  and the curve for  $\Gamma/V_0 \alpha mc_0$  by a rectangle with the same height and area. The value of  $a$  is then given by the sum of the base length of this rectangle and the quantity  $r_0/mc_0$ . This procedure was carried out and the result  $a/mc_0 = 1.545$  was obtained. In order to obtain a more complete picture of the effect of the point vortices on the aerodynamic characteristics of the wing, four different locations were chosen for the positions of the vortices, two in the  $z = 0$  plane for values of  $a/mc_0$  equal to 1.545 and 1.3, and two at a height  $h/mc_0 = 0.3$  above the  $z = 0$  plane for the same two values of  $a/mc_0$ .

From equation (100) it can easily be shown that the value of the vertical induced velocity in the  $z_1 = 0$  plane is

$$w_v = \left( \frac{\partial \phi_v}{\partial z_1} \right)_{z_1=0} = \frac{\Gamma_w}{2\pi} \left[ \frac{y_1 - a_1}{h_1^2 + (y_1 - a_1)^2} - \frac{y_1 + a_1}{h_1^2 + (y_1 + a_1)^2} \right] \quad (101)$$

The particular inversion of equation (15) that fits the present boundary conditions (see appendix B) can be written

$$\Delta v_1(y_1) = \frac{2}{\pi \sqrt{\sigma_1^2 - y_1^2}} \int_{-\sigma_1}^{\sigma_1} \frac{w(y_2)}{y_1 - y_2} \sqrt{\sigma_1^2 - y_2^2} dy_2 \quad (102)$$

Place the value of  $w_v$  given by equation (101) into equation (102) and add the condition that the tail be a flat-plate lifting surface at an angle of attack  $\alpha$ , and there results

$$\Delta v_1(y_1) = \frac{-2V_0 \alpha y_1}{\sqrt{\sigma_1^2 - y_1^2}} - \frac{\Gamma_w}{2\pi \sqrt{\sigma_1^2 - y_1^2}} \left( \frac{\sqrt{b_1^2 - \sigma_1^2}}{y_1 + b_1} + \frac{\sqrt{b_1^2 - \sigma_1^2}}{y_1 + b_1} + \frac{\sqrt{b_1^2 - \sigma_1^2}}{y_1 - b_1} + \frac{\sqrt{b_1^2 - \sigma_1^2}}{y_1 - b_1} \right) \quad (103)$$

where

$$\begin{aligned} b_1 &= a_1 + ih_1 \\ \bar{b}_1 &= a_1 - ih_1 \end{aligned} \quad (104)$$

and where the radicals are defined uniquely if the complex plane is cut along the real axis between  $-\infty$  and  $\sigma_1$ . (For example,  $\sqrt{b_1^2 - \sigma_1^2}$  can be set equal to  $\rho_1 e^{i\phi_1}$  where  $\phi_1$  must lie between  $-\pi$  and  $\pi$ .) Although the above expression for  $\Delta v$  can be put in real terms by applying the transformations

$$\begin{aligned} a_1 &= \sigma_1 \cosh \gamma_1 \cos \omega_1 \\ |h_1| &= \sigma_1 \sinh \gamma_1 \sin \omega_1 \end{aligned} \quad (105)$$

it is easier in deriving subsequent quantities from  $\Delta v_1$  to use equation (103) first and to make the transformation afterwards.

Span loading.-- The span loading can be determined from the relation

$$\Delta\phi_t = \int_{\sigma}^y \Delta v(y_2) dy_2 \quad (106)$$

where  $\Delta v$  is given by equation (103). There finally results

$$\Delta\phi_{1t} = 2V_0\alpha \sqrt{\sigma_1^2 - y_1^2} - \frac{2\Gamma_w}{\pi} \arctan \frac{\sqrt{[\sigma_1^2(\sinh^2\gamma_1 - \cos^2\omega_1) + y_1^2]^2 + 4\sigma_1^2(\sigma_1^2 - y_1^2)\sinh^2\gamma_1\cos^2\omega_1 - \sigma_1^2(\sinh^2\gamma_1 - \cos^2\omega_1) - y_1^2}}{2\sigma_1 \sqrt{\sigma_1^2 - y_1^2} \sinh \gamma_1 \cos \omega_1}, \quad (107a)$$

$$r_1^2 < y_1^2 < \sigma_1^2$$

and on the body

$$\Delta\phi_{1t} = 2V_0\alpha \left( \sqrt{\sigma_1^2 - y_1^2} - \sqrt{r_1^2 - y_1^2} \right) - \frac{2\Gamma_w}{\pi} \arctan \frac{\sqrt{[\sigma_1^2(\sinh^2\gamma_1 - \cos^2\omega_1) + y_1^2]^2 + 4\sigma_1^2(\sigma_1^2 - y_1^2)\sinh^2\gamma_1\cos^2\omega_1 - \sigma_1^2(\sinh^2\gamma_1 - \cos^2\omega_1) - y_1^2}}{2\sigma_1 \sqrt{\sigma_1^2 - y_1^2} \sinh \gamma_1 \cos \omega_1} + \frac{2\Gamma_w}{\pi} \arctan \frac{\sqrt{[r_1^2(\sinh^2\gamma_2 - \cos^2\omega_2) + y_1^2]^2 + 4r_1^2(r_1^2 - y_1^2)\sinh^2\gamma_2\cos^2\omega_2 - r_1^2(\sinh^2\gamma_2 - \cos^2\omega_2) - y_1^2}}{2r_1 \sqrt{r_1^2 - y_1^2} \sinh \gamma_2 \cos \omega_2}, \quad y_1^2 < r_1^2 \quad (107b)$$

The terms  $\sinh \gamma_1$ ,  $\sinh \gamma_2$ ,  $\sin \omega_1$ , and  $\sin \omega_2$  are all defined in the table of symbols. Equations (107a) and (107b) can, of course, be transformed to the physical plane by transforming each symbol therein from the  $\xi_1$  system to the  $\xi$  system.

The variation of the tail span loading, as given by equations (107a) and (107b), is shown in figures 2(a) and 2(b) for the various vortex positions discussed.

Chordwise load distribution.— The loading on the tail can be calculated from the relation

$$\left(\frac{\Delta p}{q\alpha}\right)_t = \frac{2}{V_0\alpha} \frac{\partial \Delta \varphi_t}{\partial x} = \frac{2}{V_0\alpha} \frac{\partial \Delta \varphi_{1t}}{\partial \sigma_1} \frac{d\sigma_1}{dx} \quad (108)$$

The value of  $\partial \Delta \varphi_{1t} / \partial \sigma_{1t}$  follows from equations (107); thus

$$\frac{\partial \Delta \varphi_{1t}}{\partial \sigma_1} = \frac{2V_0\alpha\sigma_1}{\sqrt{\sigma_1^2 - y_1^2}} \left[ 1 + \frac{\Gamma_w}{\pi} \left( \frac{1}{\sqrt{b_1^2 - \sigma_1^2}} + \frac{1}{\sqrt{b_1^2 - \sigma_1^2}} \right) \right] \quad (109)$$

Hence,

$$\left(\frac{\Delta p}{q\alpha}\right)_t = \frac{4\sigma_1}{\sqrt{\sigma_1^2 - y_1^2}} \left[ 1 - \frac{\Gamma_w \sinh \gamma_1 \cos \omega_1}{V_0\alpha\sigma_1(\sinh^2 \gamma_1 + \sin^2 \omega_1)} \right] \frac{d\sigma_1}{dx} \quad (110)$$

Equation (110) when transformed to the  $\xi$  plane gives the surface load distribution over the tail due to the presence of the two point vortices as well as the inclination of the tail to the free stream.

Total lift.— The total lift can be obtained by integrating the span loading. Thus, if  $L_t$  represents the lift on the tail,

$$\frac{L_t}{q\alpha} = \frac{2}{V_0\alpha} \int_0^\sigma \Delta \varphi_t dy \quad (111)$$

Carrying out this integration yields

$$\frac{L_t}{2q\alpha} = \pi(\sigma_1^2 - r_1^2) - \frac{2\Gamma_w}{V_0\alpha} (r_1 \sinh \gamma_2 \cos \omega_2 - \sigma_1 \sinh \gamma_1 \cos \omega_1) \quad (112)$$



This result was transformed and plotted in figures 3(a) and 3(b) for the values discussed.

Total drag.- The total drag is given by the relation

$$D_t = \alpha L_t + F_t \quad (113)$$

where  $F_t$  is the suction force on the tail leading edge. As in previous steps (see, e.g., equation (92)) the calculation of  $F_t$  depends on the evaluation of the function  $G$ . In this case  $G^2$  is

$$\frac{\alpha^2}{2\sqrt{1+\mu^2}} \sqrt{\frac{y^4-r_0^4}{y^3}} \left[ 1 - \frac{\Gamma}{2V_0\alpha\pi} \left( \frac{1}{\sqrt{b_1^2-\sigma_1^2}} + \frac{1}{\sqrt{b_1^2-\sigma_1^2}} \right) \right]^2 \quad (114)$$

The final result, in the  $\xi_1$  plane, for the total drag can be written

$$\frac{D_t}{q\alpha^2} = \pi(\sigma_1^2-r_1^2) + \frac{1}{2\pi} \left( \frac{\Gamma_w}{V_0\alpha} \right)^2 \ln \frac{(a_1^2-h_1^2-\sigma_1^2)^2+4a_1^2h_1^2+(a_1^2-h_1^2-\sigma_1^2)\sqrt{(a_1^2-h_1^2-\sigma_1^2)^2+4a_1^2h_1^2}}{(a_1^2-h_1^2-r_1^2)^2+4a_1^2h_1^2+(a_1^2-h_1^2-r_1^2)\sqrt{(a_1^2-h_1^2-r_1^2)^2+4a_1^2h_1^2}} \quad (115)$$

A plot of the drag is given in figures 4(a) and 4(b).

Chord loading.- As before, in the development of equations (97a) and (97b), for example, the chord loading can be calculated either by performing the integration  $\int (\Delta p/q\alpha)_t dy$ , or by differentiating with respect to  $x$  the total lift ( $L_t/q\alpha$ ). These two different approaches serve to check each other and both lead to the same result, namely,

$$2 \int_0^\sigma \left( \frac{\Delta p}{q\alpha} \right)_t dy = 4\pi\sigma_1 \frac{d\sigma_1}{dx} \left[ 1 - \frac{\Gamma_w \sinh \gamma_1 \cos \omega_1}{V_0\alpha\sigma_1\pi(\sinh^2\gamma_1+\sin^2\omega_1)} \right] \quad (116)$$

Center of pressure.- Results for the center of pressure  $x_{c.p.}$  (where  $x_{c.p.} = -M_t/L_t$ ) are shown in figures 5(a) and 5(b).

## CONCLUDING REMARKS

When an airplane is slender enough<sup>11</sup> (in the longitudinal sense) or is flying close enough to the speed of sound, the mathematical description of its attendant flow field is greatly simplified - so much so, in fact, that the analysis of whole wing-body-tail combinations is feasible. This simplification comes from the fact that the induced velocities in each lateral plane are completely independent of the nature of the airplane or flow field behind the reference plane and are affected by disturbances ahead only through the presence of free vortices trailing downstream from the lifting elements. In the case of a tail, these free vortices stream back from the wing trailing edge.

In this report, special wing plan forms were studied: special in that they produced flat span-loading curves between the wing tips and fuselage. For such wings, the free trailing vortices were concentrated entirely in the region directly behind the wing tips. In general, the trailing vorticity would be concentrated predominately in this region. The behavior of this trailing vortex system is bounded by the behavior of two extreme models: a vortex sheet lying everywhere in the plane of the tail, and two laterally symmetric point vortices lying in or above the plane of the tail. Each of these models was examined.

One point vortex was placed in the plane of the tail at a distance from the fuselage in the spanwise direction determined by replacing the wing-span loading curve by a rectangle of the same height. As shown by figures 2 through 5, the results for this point vortex were not significantly different from those for the vortex sheet. In either case, the presence of the trailing wing vortices reduced by about 40 percent the effectiveness of the triangular tail surface in producing lift for the range of tail spans and body diameters considered. For the same conditions the tail drag was reduced only 18 percent.

For the particular locations chosen for the point vortices, it was found that both the lift and drag decreased as the vortices moved closer to the tail. On a percentage basis the decrease was roughly the same.

---

<sup>11</sup>The assumptions underlying slender wing theory are obviously violated along lines such as the leading edge,  $x = mc_0$ , and the Mach wave from the trailing-edge-fuselage juncture,  $x = c_0$ . Along these lines the pressure gradient is discontinuous and  $(M_0^2 - 1) \phi_{xx}$  is not bounded. Similar situations appear repeatedly in the linearized analysis of aerodynamic flow phenomena and in each case agreement with experimental results cannot be anticipated.

---

The position of the center of pressure on the triangular tail was insensitive to the presence of the wing vortex system regardless of the vortex pattern chosen. In the extreme case, when the point vortices were nearest the tail, the location of the tail center of pressure with reference to the tail apex as 5 percent forward of the position obtained when the wing was absent.

Ames Aeronautical Laboratory  
National Advisory Committee for Aeronautics  
Moffett Field, Calif., Aug. 20, 1951

## APPENDIX A

## LIST OF IMPORTANT SYMBOLS

a	horizontal distance from $y=0$ plane to vortex (See sketch (z).)
$b_1$	$a_1 + ih_1$
$\bar{b}_1$	$a_1 - ih_1$
c	local chord
$c_0$	characteristic chord (See sketch (a).)
$c_d$	section drag coefficient $\left( \frac{d}{qc} \right)$
$c_l$	section lift coefficient $\left( \frac{l}{qc} \right)$
d	section drag force
D	drag force
$E_0$	complete elliptic integral of the second kind $\left( \int_0^1 \sqrt{\frac{1-k_0^2 t^2}{1-t^2}} dt \right)$
$E(k, \psi)$	incomplete elliptic integral of the second kind $\left( \int_0^\psi \sqrt{\frac{1-k^2 t^2}{1-t^2}} dt \right)$
F	suction force at leading edge of lifting surface
$F(k, \psi)$	incomplete elliptic integral of the first kind $\left( \int_0^\psi \frac{dt}{\sqrt{(1-k^2 t^2)(1-t^2)}} \right)$
h	vertical distance from $z=0$ plane to vortex (See sketch (z).)
$K_0$	complete elliptic integral of the first kind $\left( \int_0^1 \frac{dt}{\sqrt{(1-k_0^2)(1-t^2)}} \right)$
k	modulus of elliptic integrals
$k'$	$\sqrt{1-k^2}$

$k_0$	$\frac{\sqrt{(s^2 t^2 - r_0^4)(s^2 - t^2)}}{t(s^2 - r_0^2)}$
$k_1$	$k_0$ in the $\xi_1$ plane $\left( \frac{\sqrt{s_1^2 - t_1^2}}{\sqrt{s_1^2 - r_1^2}} \right)$
$k_2$	$\frac{2r_0 \sqrt{(s^2 t^2 - r_0^4)(s^2 - t^2)}}{(s^2 - r_0^2)(t^2 + r_0^2)}$
$k_3$	$k_2$ in the $\xi_1$ plane $\left( \frac{r_1 \sqrt{s_1^2 - t_1^2}}{t_1 \sqrt{s_1^2 - r_1^2}} \right)$
$k_4$	$\frac{(\sigma^2 - r_0^2) \sqrt{(s^2 - t^2)(s^2 t^2 - r_0^4)}}{(t^2 - r_0^2) \sqrt{(s^2 - \sigma^2)(s^2 \sigma^2 - r_0^4)}}$
$k_5$	$k_4$ in the $\xi_1$ plane $\left( \frac{\sqrt{(\sigma_1^2 - r_1^2)(s_1^2 - t_1^2)}}{\sqrt{(s_1^2 - \sigma_1^2)(t_1^2 - r_1^2)}} \right)$
$l$	section lift force
$L$	lift force
$m$	slope of wing leading edge (See sketch (a).)
$M$	pitching moment, positive when tail is forced down
$M_0$	free-stream Mach number
$p$	local static pressure
$\frac{\Delta p}{q}$	loading coefficient $\left( \frac{p_l - p_u}{q} \right)$
$q$	free-stream dynamic pressure $\left( \frac{1}{2} \rho_0 V_0^2 \right)$
$r_0$	radius of body (See sketch (a).)
$s$	distance from $x$ axis to wing leading edge (See sketch (a).)
$s_0$	maximum value of $s$ (See sketch (a).)
$S$	wing area
$t$	distance from $x$ axis to wing trailing edge (See sketch (a).)
$t_0$	maximum value of $t$ (See sketch (a).)

$u, v, w$	perturbation velocity components in the $x, y, z$ directions, respectively
$\Delta u, \Delta v, \Delta w$	jump in velocities across $z=0$ plane, $u_u - u_l$ , $v_u - v_l$ , $w_u - w_l$ , respectively
$v_r$	radial component of perturbation velocity in a $y, z$ plane
$V_0$	free-stream velocity
$x, y, z$	Cartesian coordinates
$x_{c.p.}$	distance to center of pressure (See sketch (w) and fig. 5.)
$\alpha$	angle of attack of airplane
$\beta$	$\sqrt{M_0^2 - 1}$
$\sinh \gamma_1$	$\frac{ h_1 }{\sigma_1 \sin \omega_1}$
$\sinh \gamma_2$	$\frac{ h_1 }{r_1 \sin \omega_2}$
$\Gamma$	total circulation about wing section $[(\Delta\Phi)_{T.E.}]$
$\eta$	$y^2$
$\theta$	polar angle in $y, z$ plane
$\Lambda_0(k, \psi)$	$\frac{2}{\pi} [KE(k', \psi) + (E-K)F(k', \psi)]$
$\mu$	slope of tail leading edge (See sketch (x).)
$\xi$	complex variable $(y+iz)$
$\rho$	polar distance in $y, z$ plane $(\sqrt{y^2+z^2})$
$\rho_0$	free-stream density
$\sigma$	distance from $x$ axis to leading edge of tail (See sketch (x).)
$\Phi$	perturbation velocity potential
$\Delta\Phi$	jump in $\Phi$ across $z=0$ plane $(\Phi_u - \Phi_l)$
$(\Delta\Phi)_{T.E.}$	value of $\Delta\Phi$ at trailing edge

$\psi$  argument of elliptic integrals

$$\psi_0 \frac{\sqrt{(s^2 y^2 - r_0^4)(s^2 - y^2)t^2}}{\sqrt{(s^2 t^2 - r_0^4)(s^2 - t^2)y^2}}$$

$$\psi_1 \quad \psi_0 \text{ in } \xi_1 \text{ plane } \left( \frac{\sqrt{s_1^2 - y_1^2}}{\sqrt{s_1^2 - t_1^2}} \right)$$

$$\psi_2 \frac{2t\sqrt{r_0^2 - y^2}}{\sqrt{(t^2 + r_0^2)^2 - 4y^2 t^2}}$$

$$\psi_3 \quad \psi_2 \text{ in } \xi_1 \text{ plane } \left( \frac{\sqrt{r_1^2 - y_1^2}}{\sqrt{t_1^2 - y_1^2}} \right)$$

$$\psi_4 \frac{s(t^2 + r_0^2)}{t(s^2 + r_0^2)}$$

$$\psi_5 \quad \psi_4 \text{ in } \xi_1 \text{ plane } \left( \frac{t_1}{s_1} \right)$$

$$\psi_6 \frac{s^2 - r_0^2}{s^2 + r_0^2}$$

$$\psi_7 \quad \psi_6 \text{ in } \xi_1 \text{ plane } \left( \frac{\sqrt{s_1^2 - r_1^2}}{s_1} \right)$$

$$\psi_8 \frac{s(t^2 - r_0^2)}{t(s^2 - r_0^2)}$$

$$\psi_9 \quad \psi_8 \text{ in } \xi_1 \text{ plane } \left( \frac{\sqrt{t_1^2 - r_1^2}}{\sqrt{s_1^2 - r_1^2}} \right)$$

$$\sin^2 \omega_1 \frac{[\sigma_1^2 - a_1^2 - h_1^2 + \sqrt{(a_1^2 + h_1^2 - \sigma_1^2)^2 + 4\sigma_1^2 h_1^2}]}{2\sigma_1^2}$$

$$\sin^2 \omega_2 \frac{[r_1^2 - a_1^2 - h_1^2 + \sqrt{(a_1^2 + h_1^2 - r_1^2)^2 + 4r_1^2 h_1^2}]}{2r_1^2}$$

#### Subscripts

- 1 complex plane resulting from the application of the Joukowski transformation to the physical plane
- 12 boundary conditions given by equations (12)
- 13 boundary conditions given by equations (13)

a        wake  
b        body  
l        lower surface of  $z=0$  plane  
n        component normal to leading edge  
t        tail  
u        upper surface of  $z=0$  plane  
v        rolled up vortex  
w        wing



## APPENDIX B

## INVERSION OF AN INTEGRAL EQUATION

The integral equation

$$f(\eta_1) = -\frac{1}{2\pi} \int_a^b \frac{\Delta v(\eta_2) d\eta_2}{\eta_1 - \eta_2} \quad (B1)$$

can be inverted by applying operational techniques. Consider the operator

$$\int_a^b \frac{h(\eta_1) d\eta_1}{\lambda - \eta_1} \quad (B2)$$

where  $h(\eta_1)$  is a function to be chosen later. Operating on both sides of equation (B1) yields

$$\int_a^b \frac{h(\eta_1) f(\eta_1) d\eta_1}{\lambda - \eta_1} = -\frac{1}{2\pi} \int_a^b d\eta_1 \int_a^b d\eta_2 \frac{\Delta v(\eta_2) h(\eta_1)}{(\eta_1 - \eta_2)(\lambda - \eta_1)} \quad (B3)$$

where the order of the integral and differential signs on the right-hand side of the equation indicates that the  $\eta_2$  integration is to be performed first.

The next step is to reverse the order of integration in the double integral term in equation (B3). Since an inherent singularity exists in the area of integration at the point  $\eta_1 = \eta_2 = \lambda$ , however, some care must be used in order to obtain this reversal. Designating by  $R(\lambda)$  the difference between the term taken first with one order of integration and then with another, thus

$$R(\lambda) = \int_a^b d\eta_1 \int_a^b d\eta_2 \frac{\Delta v(\eta_2) h(\eta_1)}{(\eta_1 - \eta_2)(\lambda - \eta_1)} - \int_a^b d\eta_2 \int_a^b d\eta_1 \frac{\Delta v(\eta_2) h(\eta_1)}{(\eta_1 - \eta_2)(\lambda - \eta_1)} \quad (B4)$$

$R(\lambda)$  can be evaluated by isolating the singularity and studying the difference only in its vicinity. Hence,

$$R(\lambda) = \lim_{\epsilon \rightarrow 0} \left[ \int_{\lambda-\epsilon}^{\lambda+\epsilon} d\eta_1 \int_{\lambda-\epsilon}^{\lambda+\epsilon} d\eta_2 \frac{\Delta v(\eta_2) h(\eta_1)}{(\eta_1 - \eta_2)(\lambda - \eta_1)} - \int_{\lambda-\epsilon}^{\lambda+\epsilon} d\eta_2 \int_{\lambda-\epsilon}^{\lambda+\epsilon} d\eta_1 \frac{\Delta v(\eta_2) h(\eta_1)}{(\eta_1 - \eta_2)(\lambda - \eta_1)} \right] \quad (B5)$$

Using the transformations  $\eta_1 = \lambda - \epsilon x_1$  and  $\eta_2 = \lambda - \epsilon x_2$ , equation (B5) can be reduced to the form

$$\begin{aligned} R(\lambda) &= \Delta v(\lambda) h(\lambda) \left[ \int_{-1}^1 dx_1 \int_{-1}^1 \frac{dx_2}{x_1(x_2 - x_1)} - \int_{-1}^1 dx_2 \int_{-1}^1 \frac{dx_1}{x_1(x_2 - x_1)} \right] \\ &= 2\Delta v(\lambda) h(\lambda) \int_0^1 \frac{dx_1}{x_1} \ln \frac{1-x_1}{1+x_1} \\ &= -\pi^2 \Delta v(\lambda) h(\lambda) \end{aligned} \quad (B6)$$

Substitute equations (B6) and (B4) into equation (B3) and there results

$$\int_a^b \frac{h(\eta_1) f(\eta_1) d\eta_1}{\lambda - \eta_1} = -\frac{1}{2\pi} \left[ -\pi^2 \Delta v(\lambda) h(\lambda) + \int_a^b \Delta v(\eta_2) d\eta_2 \int_a^b \frac{h(\eta_1) d\eta_1}{(\eta_1 - \eta_2)(\lambda - \eta_1)} \right]$$

or

$$\Delta v(\lambda) = \frac{2}{\pi h(\lambda)} \left[ \frac{1}{2\pi} \int_a^b \Delta v(\eta_2) d\eta_2 \int_a^b \frac{h(\eta_1) d\eta_1}{(\eta_1 - \eta_2)(\lambda - \eta_1)} + \int_a^b \frac{h(\eta_1) f(\eta_1) d\eta_1}{\lambda - \eta_1} \right] \quad (B7)$$

If  $h(\eta_1) = \sqrt{(b - \eta_1)(\eta_1 - a)}$  equation (B7) becomes

$$\Delta v(\lambda) = \frac{2}{\pi \sqrt{(b - \lambda)(\lambda - a)}} \left[ \frac{1}{2} \int_a^b \Delta v(\eta_2) d\eta_2 + \int_a^b \frac{f(\eta_1) \sqrt{(b - \eta_1)(\eta_1 - a)}}{\lambda - \eta_1} d\eta_1 \right] \quad (B8)$$

Since, however, equation (B8) contains both  $\Delta v$  and its integral, it does not represent a unique solution for  $\Delta v$ . In order to obtain a unique solution, some additional condition must be imposed. If this condition is that  $\Delta v(a) = 0$ , then the proper choice of  $h(\eta_1)$  in equation (B7) is

$$h(\eta_1) = \sqrt{\frac{\eta_1 - a}{b - \eta_1}}$$

which leads immediately to the unique result

$$\Delta v(\lambda) = \frac{2}{\pi} \sqrt{\frac{\lambda - a}{b - \lambda}} \int_a^b \frac{f(\eta_1) d\eta_1}{\lambda - \eta_1} \sqrt{\frac{b - \eta_1}{\eta_1 - a}} \quad (B9)$$

## REFERENCES

1. Jones, R. T.: Properties of Low-Aspect-Ratio Pointed Wings at Speeds Below and Above the Speed of Sound. NACA Rep. 835, 1946. (Formerly NACA TN 1032).
2. Heaslet, Max. A., Lomax, Harvard, and Spreiter, John R.: Linearized Compressible-Flow Theory for Sonic Flight Speeds. NACA Rep. 956, 1950. (Formerly NACA TN 1824)
3. Spreiter, John R.: Aerodynamic Properties of Slender Wing-Body Combinations at Subsonic, Transonic, and Supersonic Speeds. NACA Rep. 962, 1948. (Formerly NACA TN's 1662 and 1897)
4. Lomax, Harvard, and Heaslet, Max. A.: Linearized Lifting-Surface Theory for Swept-Back Wings with Slender Plan Forms. NACA TN 1992, 1949.
5. Heaslet, Max. A., and Lomax, Harvard: The Application of Green's Theorem to the Solution of Boundary-Value Problems in Linearized Supersonic Wing Theory. NACA Rep. 961, 1950. (Formerly NACA TN 1767)
6. Cohen, Doris: The Theoretical Lift of Flat Swept-Back Wings at Supersonic Speeds. NACA TN 1555, 1948.
7. Cohen, Doris: Theoretical Loading at Supersonic Speeds of Flat Swept-Back Wings with Interacting Trailing and Leading Edges. NACA TN 1991, 1949.
8. Brown, Clinton E.: Theoretical Lift and Drag of Thin Triangular Wings at Supersonic Speeds. NACA Rep. 839, 1946.
9. Heuman, Carl: Tables of Complete Elliptic Integrals. Journal of Mathematics and Physics, v. 20, 1941, pp. 127-206.
10. Spreiter, John R., and Sacks, Alvin H.: The Rolling Up of the Trailing Vortex Sheet and its Effect on the Downwash Behind Wings. Jour. of the Aero. Sci., vol. 18, January 1951, pp. 21-32.

TABLE I.- POSITION OF TRAILING EDGE

$r_o/mc_o =$	0	0.100	0.224	0.316	0.447	0.500	0.600	0.700	0.800	0.900
$x/c_o$	$y/mc_o$	$y/mc_o$	$y/mc_o$	$y/mc_o$	$y/mc_o$	$y/mc_o$	$y/mc_o$	$y/mc_o$	$y/mc_o$	$y/mc_o$
1.00	0	0.100	0.224	0.316	0.447	0.500	0.600	0.700	0.800	0.900
1.05	.168	.213	.323	.413	.542	.593	.690	.791	.883	.970
1.10	.256	.290	.387	.473	.598	.649	.746	.844	.933	1.020
1.15	.332	.361	.447	.526	.648	.699	.796	.890	.982	1.067
1.20	.400	.425	.504	.579	.698	.748	.845	.933	1.031	1.113
1.30	.526	.545	.614	.682	.797	.845	.941	1.028	1.126	1.213
1.40	.644	.661	.721	.786	.896	.941	1.033	1.123	1.221	1.312
1.50	.756	.773	.826	.888	.993	1.036	1.128	1.217	1.315	1.410
1.60	.867	.884	.931	.990	1.090	1.130	1.222	1.312	1.412	1.506
1.80	1.083	1.096	1.140	1.192	1.283	1.323	1.413	1.504	1.606	1.703
2.00	1.297	1.308	1.394	1.393	1.482	1.522	1.610	1.700	1.800	1.800
2.20	1.507	1.516	1.555	1.596	1.676	1.723	1.803	1.893	1.996	2.100
2.60	1.91	1.92	1.96	2.00	2.07	2.12	2.20	2.29	2.39	2.50
3.00	2.32	2.33	2.37	2.40	2.47	2.52	2.60	2.69	2.79	2.90
3.50	2.83	2.84	2.87	2.91	2.98	3.02	3.10	3.19	3.29	3.39
4.00	3.33	3.34	3.38	3.41	3.49	3.52	3.60	3.69	3.78	3.89



TABLE II.- VALUES OF LOCAL CHORD

$r/mc_0 =$	0	0.100	0.224	0.316	0.447	0.500	0.600	0.700	0.800	0.900
$y/mc_0$	$c/c_0$	$c/c_0$	$c/c_0$	$c/c_0$	$c/c_0$	$c/c_0$	$c/c_0$	$c/c_0$	$c/c_0$	$c/c_0$
0	1.000	- - -	- - -	- - -	- - -	- - -	- - -	- - -	- - -	- - -
.100	.926	0.900	- - -	- - -	- - -	- - -	- - -	- - -	- - -	- - -
.227	.910	.831	0.776	- - -	- - -	- - -	- - -	- - -	- - -	- - -
.316	.826	.802	.732	0.684	- - -	- - -	- - -	- - -	- - -	- - -
.447	.790	.772	.703	.633	0.553	- - -	- - -	- - -	- - -	- - -
.500	.777	.761	.695	.627	.522	0.500	- - -	- - -	- - -	- - -
.600	.760	.746	.685	.620	.504	.462	0.400	- - -	- - -	- - -
.700	.748	.735	.679	.617	.498	.451	.362	0.300	- - -	- - -
.8	.738	.724	.673	.614	.500	.452	.355	.262	0.200	- - -
.9	.728	.715	.668	.612	.503	.459	.358	.260	.170	0.100
1.0	.722	.709	.665	.610	.505	.464	.365	.269	.170	.082
1.1	.719	.704	.661	.608	.508	.468	.372	.278	.175	.079
1.2	.708	.697	.658	.607	.512	.472	.376	.285	.180	.081
1.3	.703	.692	.653	.606	.515	.475	.381	.290	.185	.087
1.4	.699	.688	.651	.605	.518	.477	.385	.294	.189	.094
1.6	.692	.682	.645	.603	.522	.480	.392	.299	.196	.098
1.8	.687	.677	.642	.601	.524	.481	.396	.302	.200	.100
2.0	.682	.672	.639	.599	.525	.482	.398	.305	.204	.100
2.5	.674	.663	.631	.595	.522	.484	.403	.311	.212	.101
3.0	.669	.657	.625	.593	.519	.485	.406	.315	.218	.102
4.0	.660	.648	.613	.592	.514	.485	.410	.318	.225	.102



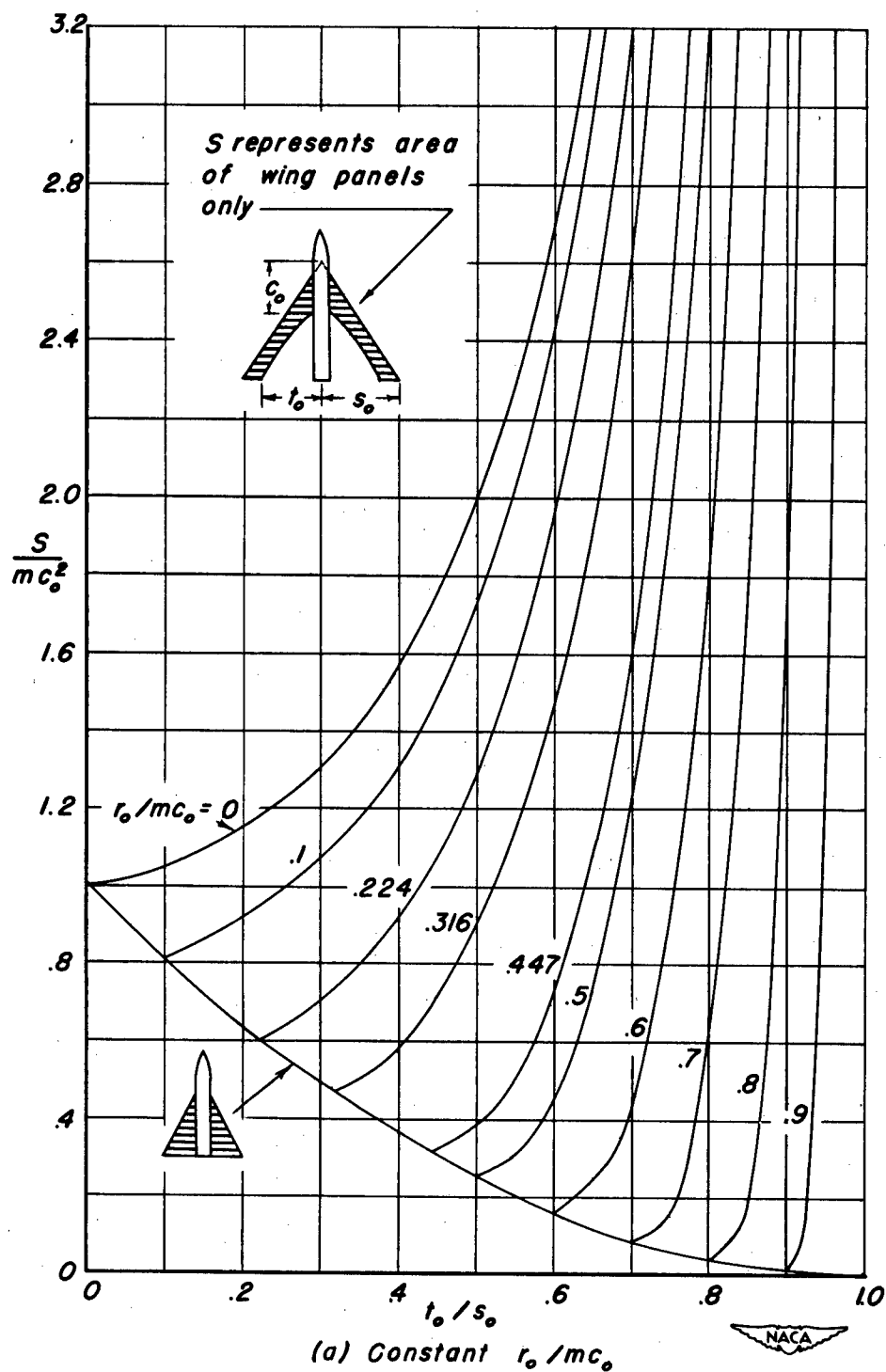
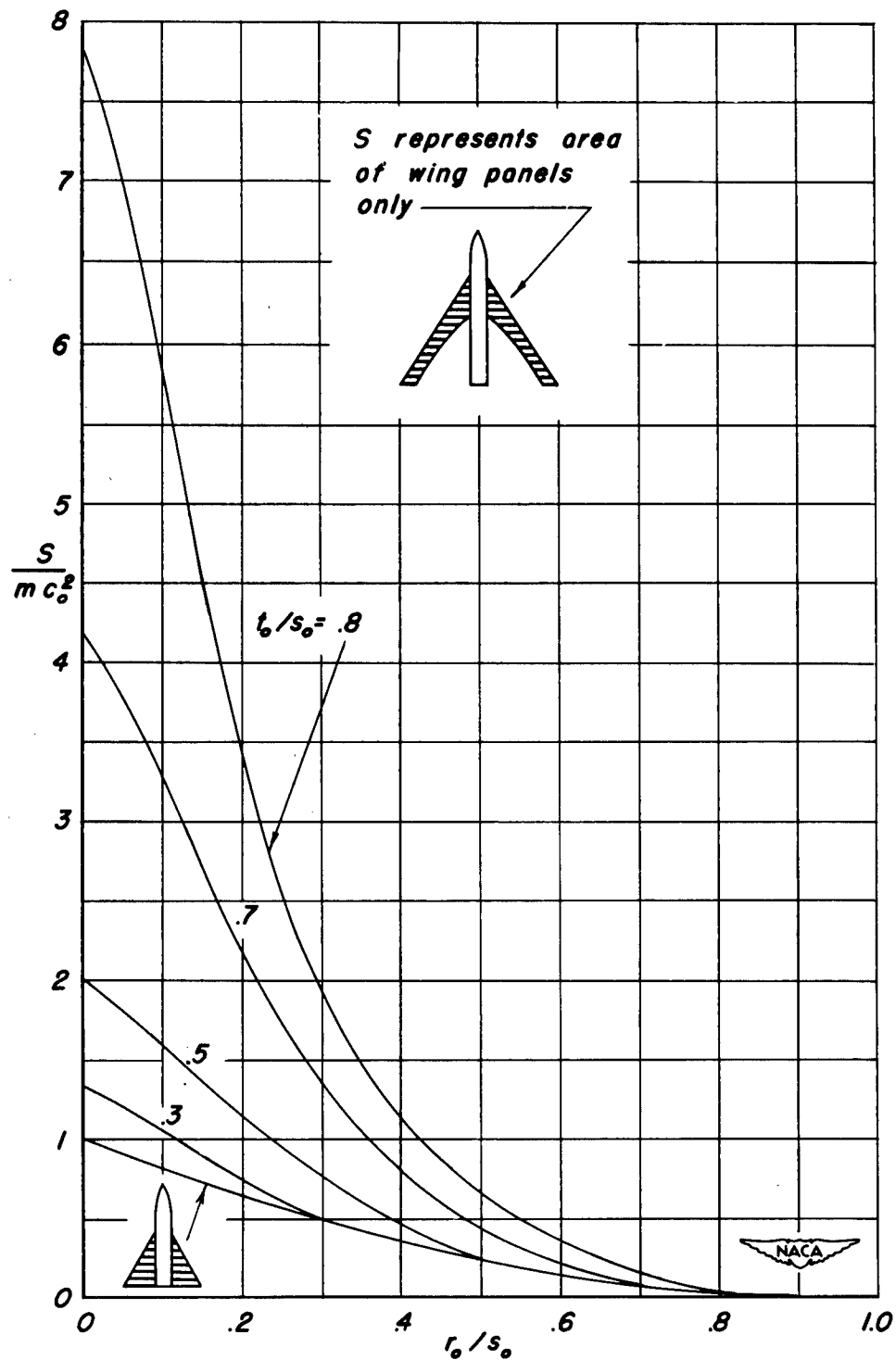


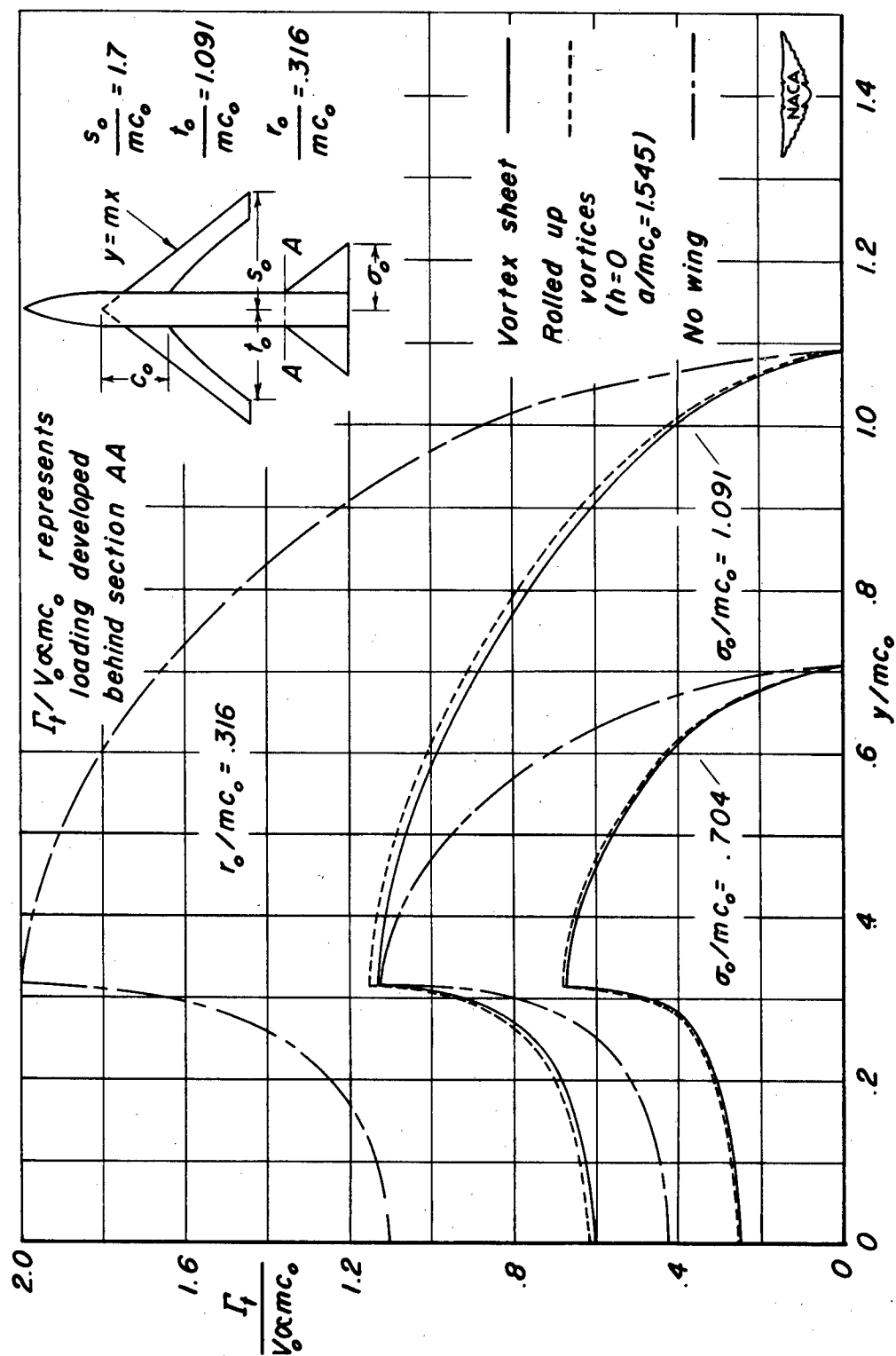
Figure 1.- Relations between the wing area, wing span, and body diameter.



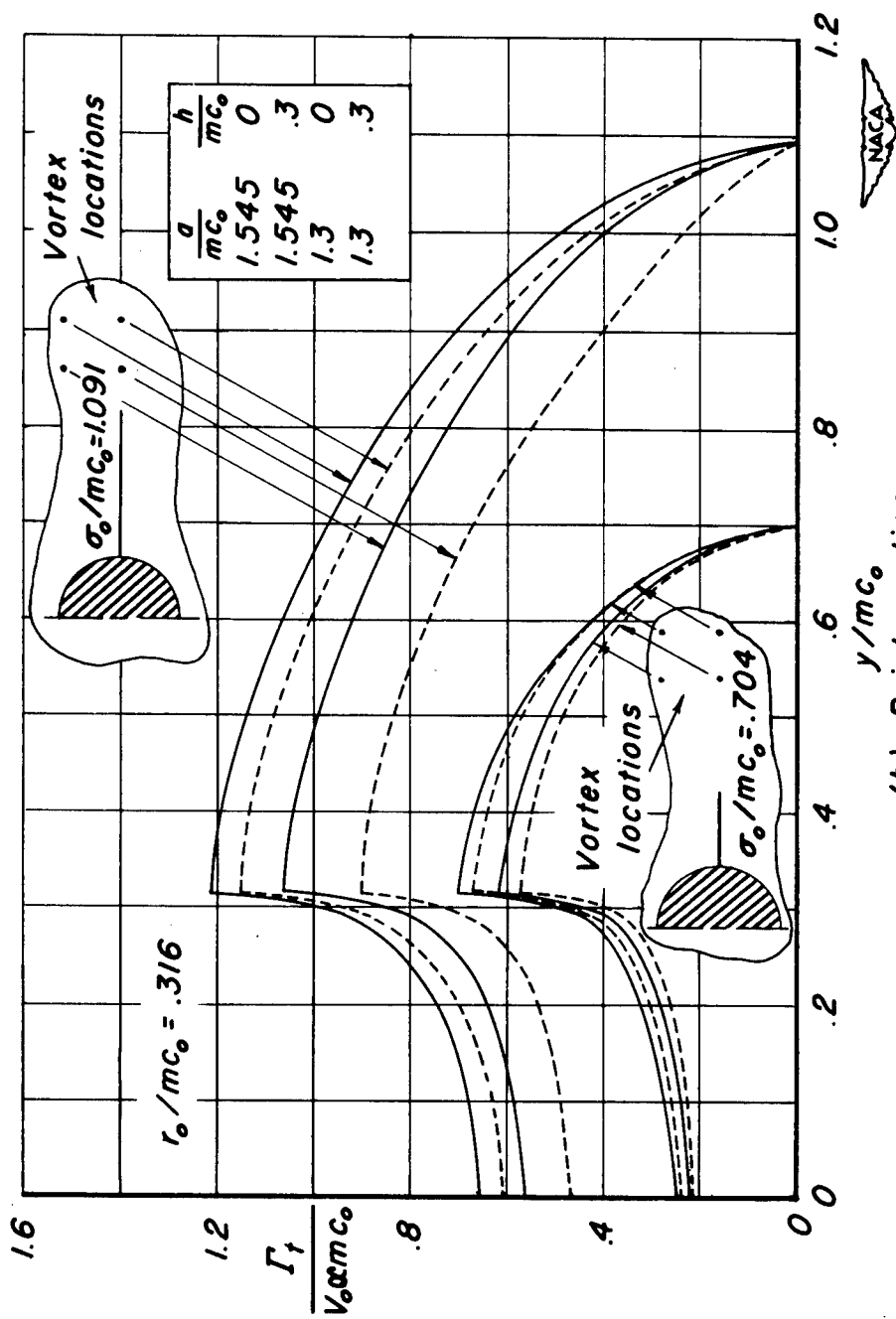
(b) Constant  $t_o/s_o$ .

Figure 1. - Concluded.



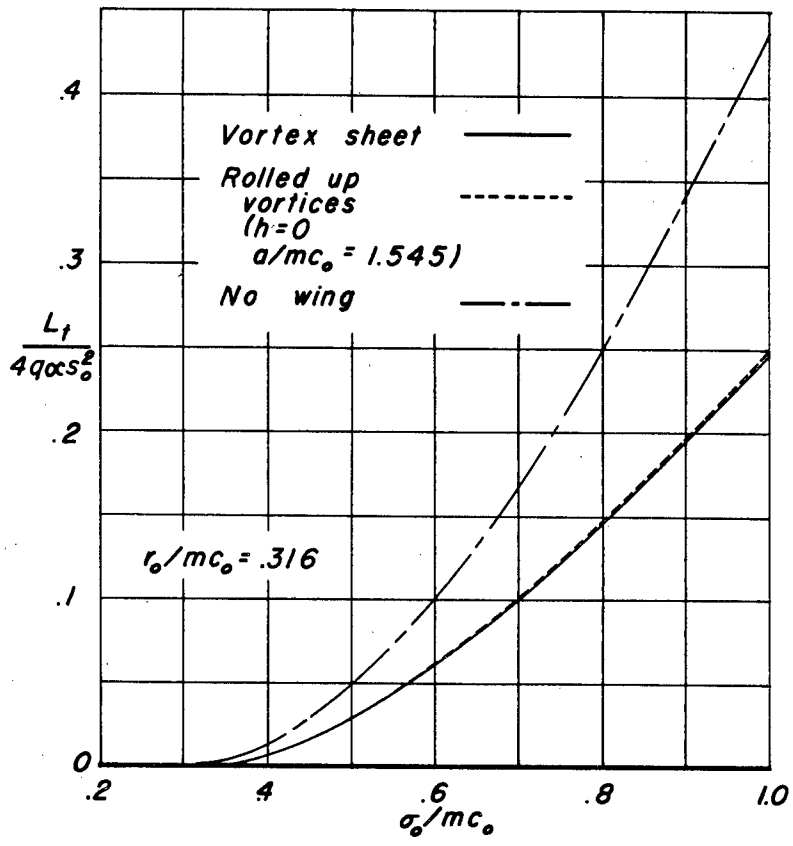


(a) Vortex sheet.  
 Figure 2.— Variation of the span loading on the tail.

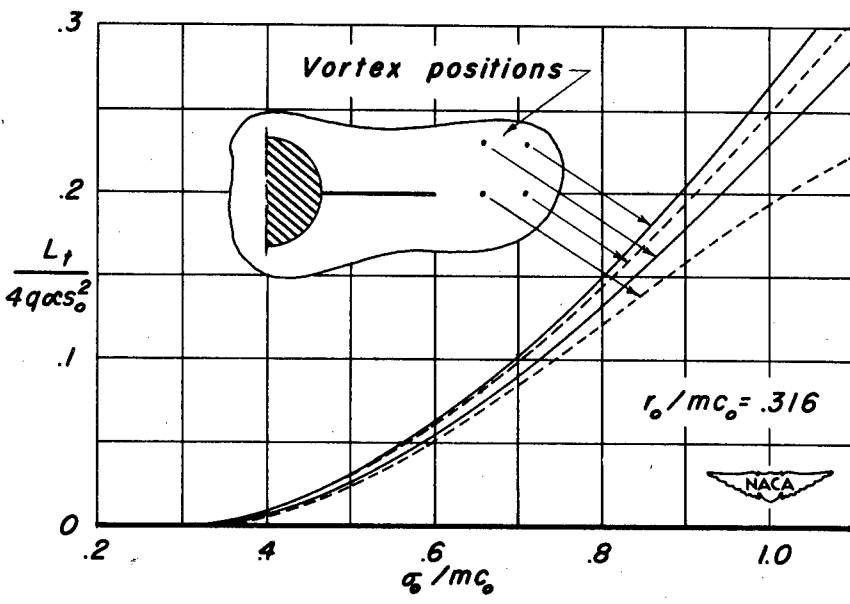


(b) Point vortices.

Figure 2. - Concluded.

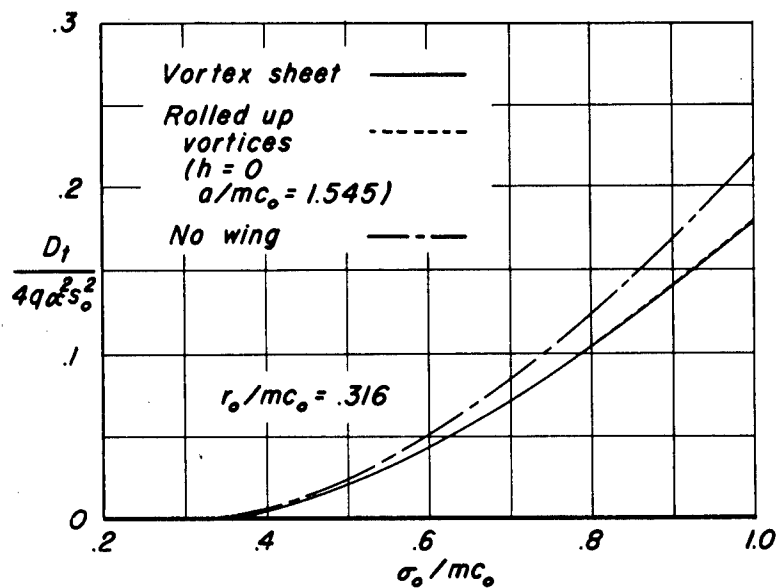


(a) Vortex sheet.

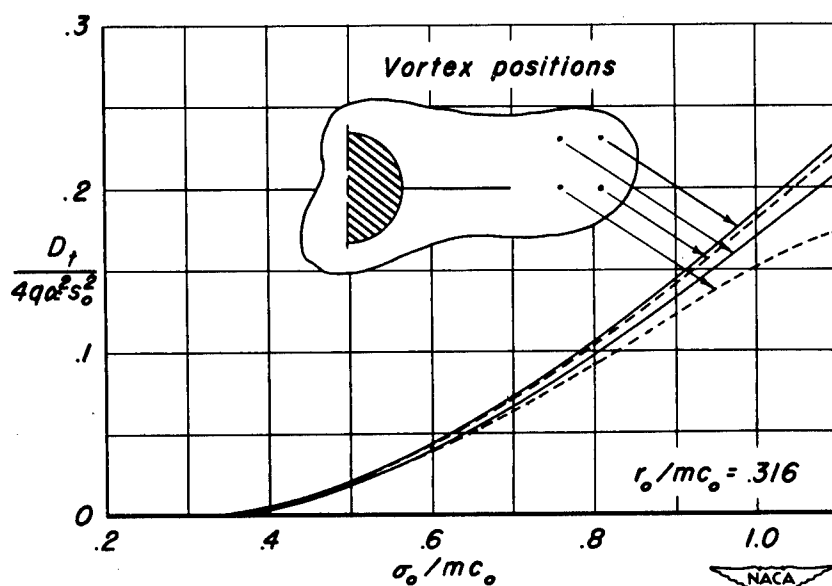


(b) Point vortices.

Figure 3.- Variation of the lift on the tail.

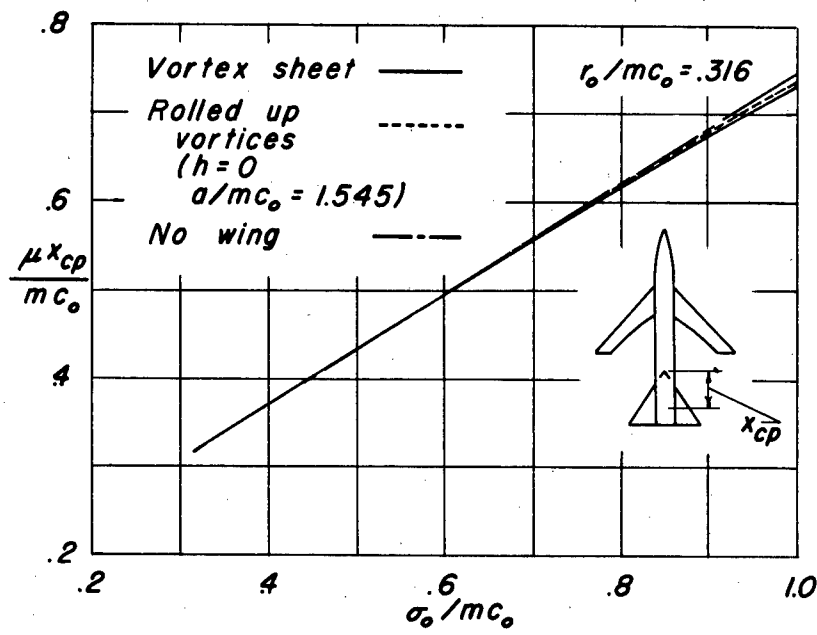


(a) Vortex sheet.

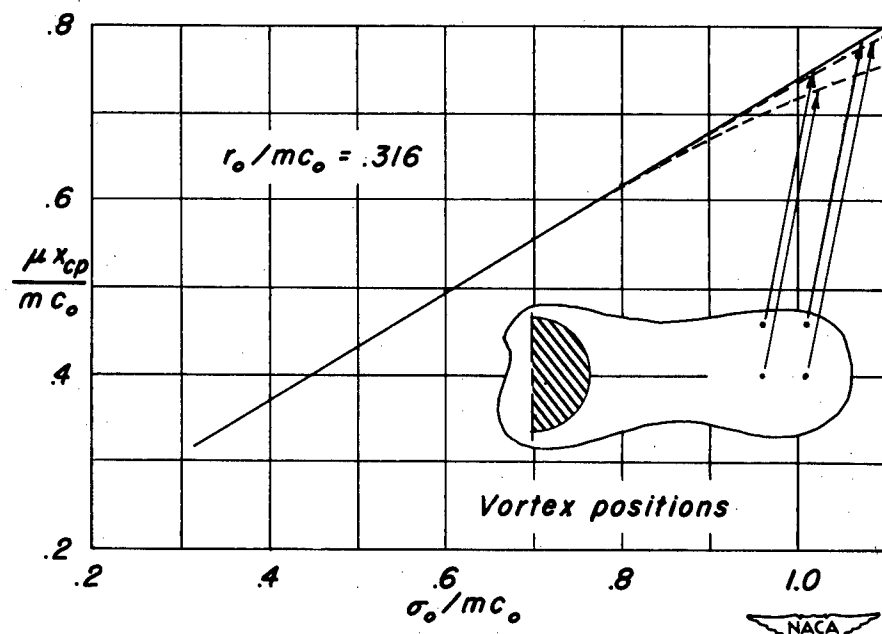


(b) Point vortices.

Figure 4. - Variation of the drag on the tail.






(a) Vortex sheet.



(b) Point vortices.

Figure 5.-Variation of the center of pressure location on the tail.

<p>NACA TN 2554 National Advisory Committee for Aeronautics. <b>THEORETICAL AERODYNAMIC CHARACTERISTICS OF A FAMILY OF SLENDER WING-TAIL-BODY COMBINATIONS.</b> Harvard Lomax and Paul F. Byrd. November 1951. 75p. diagrs., 2 tabs. (NACA TN 2554)</p> <p>The aerodynamic characteristics of an airplane configuration composed of a swept-back, nearly constant chord wing and a triangular tail mounted on a cylindrical body are presented. The analysis is based on the assumption that the free-stream Mach number is near unity or that the configuration is slender. The calculations for the tail are made on the assumption that the vortex system trailing back from the wing is either a sheet lying entirely in the plane of the flat tail surface or has completely "rolled up" into two point vortices that lie either in, above, or below the plane of the tail surface.</p> <p>Copies obtainable from NACA, Washington</p>	<ol style="list-style-type: none"> <li>1. Wings, Complete - Theory (1.2.2.1)</li> <li>2. Wings, Complete - Sweep (1.2.2.2.3)</li> <li>3. Tail-Wing-Fuselage Combinations - Airplanes (1.7.1.1.3)</li> <li>4. Wing-Tail-Body Combinations - Missiles (1.7.2.1.4)</li> </ol> <ol style="list-style-type: none"> <li>I. Lomax, Harvard</li> <li>II. Byrd, Paul F.</li> <li>III. NACA TN 2554</li> </ol> 	<p>NACA TN 2554 National Advisory Committee for Aeronautics. <b>THEORETICAL AERODYNAMIC CHARACTERISTICS OF A FAMILY OF SLENDER WING-TAIL-BODY COMBINATIONS.</b> Harvard Lomax and Paul F. Byrd. November 1951. 75p. diagrs., 2 tabs. (NACA TN 2554)</p> <p>The aerodynamic characteristics of an airplane configuration composed of a swept-back, nearly constant chord wing and a triangular tail mounted on a cylindrical body are presented. The analysis is based on the assumption that the free-stream Mach number is near unity or that the configuration is slender. The calculations for the tail are made on the assumption that the vortex system trailing back from the wing is either a sheet lying entirely in the plane of the flat tail surface or has completely "rolled up" into two point vortices that lie either in, above, or below the plane of the tail surface.</p> <p>Copies obtainable from NACA, Washington</p>	<ol style="list-style-type: none"> <li>1. Wings, Complete - Theory (1.2.2.1)</li> <li>2. Wings, Complete - Sweep (1.2.2.2.3)</li> <li>3. Tail-Wing-Fuselage Combinations - Airplanes (1.7.1.1.3)</li> <li>4. Wing-Tail-Body Combinations - Missiles (1.7.2.1.4)</li> </ol> <ol style="list-style-type: none"> <li>I. Lomax, Harvard</li> <li>II. Byrd, Paul F.</li> <li>III. NACA TN 2554</li> </ol> 
<p>NACA TN 2554 National Advisory Committee for Aeronautics. <b>THEORETICAL AERODYNAMIC CHARACTERISTICS OF A FAMILY OF SLENDER WING-TAIL-BODY COMBINATIONS.</b> Harvard Lomax and Paul F. Byrd. November 1951. 75p. diagrs., 2 tabs. (NACA TN 2554)</p> <p>The aerodynamic characteristics of an airplane configuration composed of a swept-back, nearly constant chord wing and a triangular tail mounted on a cylindrical body are presented. The analysis is based on the assumption that the free-stream Mach number is near unity or that the configuration is slender. The calculations for the tail are made on the assumption that the vortex system trailing back from the wing is either a sheet lying entirely in the plane of the flat tail surface or has completely "rolled up" into two point vortices that lie either in, above, or below the plane of the tail surface.</p> <p>Copies obtainable from NACA, Washington</p>	<ol style="list-style-type: none"> <li>1. Wings, Complete - Theory (1.2.2.1)</li> <li>2. Wings, Complete - Sweep (1.2.2.2.3)</li> <li>3. Tail-Wing-Fuselage Combinations - Airplanes (1.7.1.1.3)</li> <li>4. Wing-Tail-Body Combinations - Missiles (1.7.2.1.4)</li> </ol> <ol style="list-style-type: none"> <li>I. Lomax, Harvard</li> <li>II. Byrd, Paul F.</li> <li>III. NACA TN 2554</li> </ol> 	<p>NACA TN 2554 National Advisory Committee for Aeronautics. <b>THEORETICAL AERODYNAMIC CHARACTERISTICS OF A FAMILY OF SLENDER WING-TAIL-BODY COMBINATIONS.</b> Harvard Lomax and Paul F. Byrd. November 1951. 75p. diagrs., 2 tabs. (NACA TN 2554)</p> <p>The aerodynamic characteristics of an airplane configuration composed of a swept-back, nearly constant chord wing and a triangular tail mounted on a cylindrical body are presented. The analysis is based on the assumption that the free-stream Mach number is near unity or that the configuration is slender. The calculations for the tail are made on the assumption that the vortex system trailing back from the wing is either a sheet lying entirely in the plane of the flat tail surface or has completely "rolled up" into two point vortices that lie either in, above, or below the plane of the tail surface.</p> <p>Copies obtainable from NACA, Washington</p>	<ol style="list-style-type: none"> <li>1. Wings, Complete - Theory (1.2.2.1)</li> <li>2. Wings, Complete - Sweep (1.2.2.2.3)</li> <li>3. Tail-Wing-Fuselage Combinations - Airplanes (1.7.1.1.3)</li> <li>4. Wing-Tail-Body Combinations - Missiles (1.7.2.1.4)</li> </ol> <ol style="list-style-type: none"> <li>I. Lomax, Harvard</li> <li>II. Byrd, Paul F.</li> <li>III. NACA TN 2554</li> </ol> 